

# New insights into foreground analysis of the WMAP five-year data using FASTICA

M. Bottino<sup>1\*</sup>, A. J. Banday<sup>2,1</sup>, D. Maino<sup>3</sup>

<sup>1</sup> *Max-Planck Institute für Astrophysik, Karl-Schwarzschild Str. 1, D-85748, Garching, Germany*

<sup>2</sup> *Centre d'Etude Spatiale des Rayonnements, 9, av du Colonel Roche, BP 44346, 31028 Toulouse Cedex 4, France*

<sup>3</sup> *Dipartimento di Fisica, Università di Milano, Via Celoria 16, I-20133, Milano, Italy*

8 June 2018

## ABSTRACT

In this paper, we present a foreground analysis of the *WMAP* 5-year data using the FASTICA algorithm, improving on the treatment of the *WMAP* 3-year data in Bottino et al. (2008).

We determine coupling coefficients between the *WMAP* data and templates commonly used to trace the dominant foreground emissions, and use them to study the spectral properties of the diffuse emissions and subsequently to clean the data. We confirm the dependence of the values of these scaling factors on the extension of the mask used in the analysis and we again demonstrate some anomalies when the *Kp0* mask is adopted that remain unexplained.

We also revisit the nature of the free-free spectrum with the emphasis on attempting to confirm or otherwise the spectral feature claimed in Dobler et al. (2008b) and explained in terms of spinning dust emission in the warm ionised medium. With the application of different Galactic cuts, the index is always flatter than the canonical value of 2.14 except for the *Kp0* mask which is steeper. Irrespective of this, we can not confirm the presence of any feature in the free-free spectrum.

We experiment with a more extensive approach to the cleaning of the data, introduced in connection with the iterative application of FASTICA. We confirm the presence of a residual foreground whose spatial distribution is concentrated along the Galactic plane, with pronounced emission near the Galactic center. This is consistent with the *WMAP* haze detected in Finkbeiner et al. (2004).

Finally, we attempted to perform the same analysis on full-sky maps. The code returns good results even for those regions where the cross-talk among the components is high. However, slightly better results in terms of the possibility of reconstructing a full-sky CMB map, are achieved with a simultaneous analysis of both the five *WMAP* maps and foreground templates. Nonetheless, some residuals are still present and detected in terms of an excess in the CMB power spectrum, on small angular scales. Therefore, a minimal mask for the brightest regions of the plane is necessary, and has been defined.

**Key words:** methods: data analysis – techniques: image processing – cosmic microwave background.

\* E-mail: bottino@mpa-garching.mpg.de

## 1 INTRODUCTION

The most recent release of five years of observations from the *WMAP*<sup>1</sup> satellite again allows a quantitative improvement in studies of the Cosmic Microwave Background (CMB) for cosmological purposes. However, such an improvement requires an analogous refinement in both our understanding of local astrophysical foregrounds and in the methods employed for the separation of these components from the CMB emission.

The most evident source of foreground contamination in the *WMAP* data on at least large-angular scales is associated with the radiation produced by our own Galaxy – due to synchrotron emission, free-free emission (or *thermal bremsstrahlung*) and thermal dust emission. The presence of an additional component is now also almost universally accepted – this emission is strongly correlated with dust emission at microwave wavelengths but with a spectral dependence that is inconsistent with the basic thermal mechanism. It is generally referred to as *anomalous dust emission* since its nature is still not unambiguously identified. Finally, a subject of ongoing debate is the so-called ‘*WMAP haze*’ which Dobler et al. (2008a) attribute to *hard* synchrotron emission distributed around the Galactic Center, again with uncertain physical origin.

Many different techniques have been developed in order to clean the CMB data and subsequently study the foreground emission components. An inexhaustive selection of these includes: linear combination methods (Bennett et al. 2003; Tegmark et al. 2003; Park et al. 2007; Kim et al. 2008; Delabrouille et al. 2008), Gibbs sampling (Eriksen et al. 2008), the Maximum Entropy Method (MEM) (Bennett et al. 2003; Hinshaw et al. 2007), WIFIT (Hansen et al. 2006), Correlated Component Analysis (CCA) (Bonaldi et al. 2007), and SMICA (Delabrouille et al. 2003; Patanchon et al. 2005; Cardoso et al. 2008). In addition, an implementation of the *Independent Component Analysis* approach (Hyvärinen 1999; Hyvärinen & Oja 2000) referred to as FASTICA has been successfully applied to the problem in Maino et al. (2002) and Baccigalupi et al. (2004).

The aim of the current work is to undertake the foreground analysis of the *WMAP* 5-year data with this algorithm, as previously applied to the *WMAP* 3-year data (Bottino et al. 2008). As before, we focus on the diffuse Galactic foreground components and their spectral and spatial properties. Specifically, we first apply FASTICA to a set of data comprising one of the *WMAP* frequency maps together with three standard templates of the diffuse Galactic emission, as described in section 3 and section 5. We derive coupling coefficients for each frequency that, when used to scale the template amplitudes, are interpreted as the amount of foreground contamination for each foreground component at that frequency. Then, we iteratively apply the algorithm to the set of data, cleaned according to these scale factors. This second step of the analysis allows us to identify physical residuals that are not uniquely identified with one of the three templates.

Novel aspects of the analysis introduced in this paper include:

- consideration of the new KQ85 and KQ75 masks introduced by the *WMAP* science team with the 5-year data release
- an investigation into the connection between the mask applied to derive the coupling coefficients and the residuals resulting from the iterative multi-frequency analysis when these coefficients are applied, itself as a function of applied mask
- an attempt to understand the physical nature of the residuals revealed by the iterative analysis.
- the definition of a minimal mask that supports accurate foreground removal

A general summary of the paper is as follows. After a brief review in section 2 on how we use FASTICA to perform the analysis, in section 3 we describe the data and templates adopted, pointing out the main differences with respect to previous work. Then, in section 4 we calibrate the performance of the method using Monte Carlo simulations and by comparison to a simpler  $\chi^2$ -based method. In section 5, we present the results of the template fits, and study the spectral behaviour of the foregrounds with particular emphasis on the free-free emission. The scaled templates are then used to clean the data, the resultant properties of which are investigated in section 6. In subsequent sections the iterative application of FASTICA then attempts to improve the removal of foreground contamination from the data. Finally, we experiment with full-sky analysis, which benefits from the simultaneous analysis of multi-frequency data and templates. Section 10 summarises our main conclusions.

## 2 FASTICA AND ITS USE FOR FOREGROUND COMPONENT STUDIES

We apply FASTICA to the *WMAP* 5-year data as described in Bottino et al. (2008). We refer explicitly to that paper and to Maino et al. (2007) for details about how the code works, particularly in the context of template fitting. Nevertheless, we remind the reader that the algorithm determines a linear transformation of the input maps by seeking the maxima of their *neg-entropy*. In the implementation used here, this quantity is generally approximated by three non-linear functions, i.e.  $p(u) = u^3$ ,  $t(u) = \tanh(u)$  and  $g(u) = u \exp(-u^2)$  where  $u$  are the principal component projected data (Hyvärinen 1999; Hyvärinen & Oja 2000). Generally,  $p$ , which corresponds to the kurtosis, should be used for sub-Gaussian components but it

<sup>1</sup> *Wilkinson Microwave Anisotropy Probe*

is strongly sensitive to outliers in the distributions;  $g$  is for super-Gaussian signals while  $t$  is a general purpose function. The suitability of these functions for our purposes are described in section 4.

As before, we also compare our analysis to the simpler  $\chi^2$ -based template fitting scheme, commonly used in the field, as a convenient point of reference for our results (see Bottino et al. (2008) for details). To be consistent with the FASTICA analysis, we did not impose any constraints on the data, although this is possible as described in Hinshaw et al. (2007) and Gold et al. (2009).

The computed scaling factors are then used to clean the *WMAP* data from the estimated Galactic contaminations. The resultant maps still show evidence of residuals due to the imperfect correlation of the true foreground emission at microwave frequencies with the adopted templates, arising in part from the assumption of a fixed spectral index for each physical foreground component over the analysed sky coverage. As shown in the analysis of the *WMAP* 3-year data, a subsequent iterative application of the FASTICA algorithm to this multi-frequency pre-cleaned microwave data can yield an improved estimate of the CMB sky, plus component maps that represent foreground residuals.

### 3 DATA USED IN THE ANALYSIS

Our primary data set consists of the *WMAP* 5-year maps improved in sensitivity and precision as described in Hinshaw et al. (2009), and available for download on the LAMBDA website<sup>2</sup> in a HEALPix<sup>3</sup> pixelisation scheme, with a pixel resolution parameter of  $N_{side} = 512$ .

In our analysis, we assume that the data can be well described by a superposition of the CMB anisotropy plus foreground emission traced by three templates. These templates, suitably scaled to each frequency, are considered to represent four different physical components: synchrotron, free-free and thermal dust emission, together with the anomalous dust component – a dust correlated emission whose detailed nature is not well known, except for the fact that its contribution increases with decreasing frequency below  $\sim 61$  GHz. Evidence of a turn-over in the spectrum below  $\sim 15$  GHz may be evidence that the emission arises from so-called ‘spinning dust’ (Draine et al. 1998b). Irrespective of its detailed physical origins, its existence is generally accepted and observed in many independent analyses.

The templates are based on maps produced from independent observations of the sky at frequencies where only one emission mechanism dominates. In practise, we retain the set of templates used for the *WMAP* 3-year analysis, in order to be able to relate all changes in the analysis results to the improvements in the *WMAP* data. Therefore, we used the 408 MHz radio continuum all-sky map of Haslam et al. (1982) which is dominated by synchrotron emission away from the Galactic plane. The all-sky H $\alpha$ -map, produced by Finkbeiner et al. (2003) by assembling data from several surveys, is the template utilised for the free-free emission. The map was not corrected for dust absorption, assuming it to be negligible as suggested by Banday et al. (2003). Nevertheless, we tested the dependence of our results to this correction applied on the template. Moreover, we have also tested an alternative H $\alpha$ -map provided by Dickinson et al. (2003). This has demonstrated some differences in correlation properties with the *WMAP* data in previous analyses (Davies et al. 2006), but we do not find any sensitivity to the choice of H $\alpha$  template in our work.

Finally, we used the model for thermal dust emission at 94 GHz developed by Finkbeiner et al. (1999) (FDS) based on the *COBE*-DIRBE 100 and 240  $\mu\text{m}$  maps as calibrated by the *COBE*-FIRAS spectral data in the range 0.14 to 3.0 mm. This template was also used for the anomalous dust emission. More detailed descriptions of these foregrounds and the corresponding templates may be found, for example, in Davies et al. (2006). However, we note that the synchrotron emission (in antenna temperature) is generally described by a power-law spectrum  $T_s(\nu) \sim \nu^{-\beta_s}$ , similarly the free-free by  $T_{ff} \sim \nu^{-\beta_{ff}}$ , and the thermal dust approximated as  $T_d \sim \nu^{\beta_d}$  over the *WMAP* range of frequencies.

Of course, as noted in our previous paper, the choice of templates may not necessarily be the optimal one, although the maps utilised are those most frequently used in the literature. Indeed, Ysard et al. (2009) claim to have found evidence that the anomalous emission is preferentially correlated with the IRAS 12  $\mu\text{m}$  maps. However, in the specific case of the synchrotron emission, the *WMAP* team have suggested that the 408 MHz survey is significantly in error at microwave wavelengths, and proposed that a more realistic description of the synchrotron sky is provided by the difference of their K- and Ka-band data (Hinshaw et al. 2007). We therefore also include this template as an alternative in our analysis.

These templates are used to fit the spectral behaviour of the *WMAP* data at each frequency of observation from  $\sim 23$  GHz (K-band) up to  $\sim 94$  GHz (W-band). Where multiple samples are available at a given frequency, we have coadded them into a single sky map using uniform and equal weights. As before, we performed our analysis on sky maps convolved from their original resolution to an effective  $1^\circ$  Gaussian beam. Finally, we converted the *WMAP* data from thermodynamic temperature to brightness (antenna) temperature units, which is more natural for an analysis of foreground spectral behaviour.

Since regions close to the Galactic plane are the most seriously contaminated by foregrounds and the spectral and spatial

<sup>2</sup> Legacy Archive for Microwave Background Data Analysis – <http://lambda.gsfc.nasa.gov/>.

<sup>3</sup> <http://healpix.jpl.nasa.gov>.

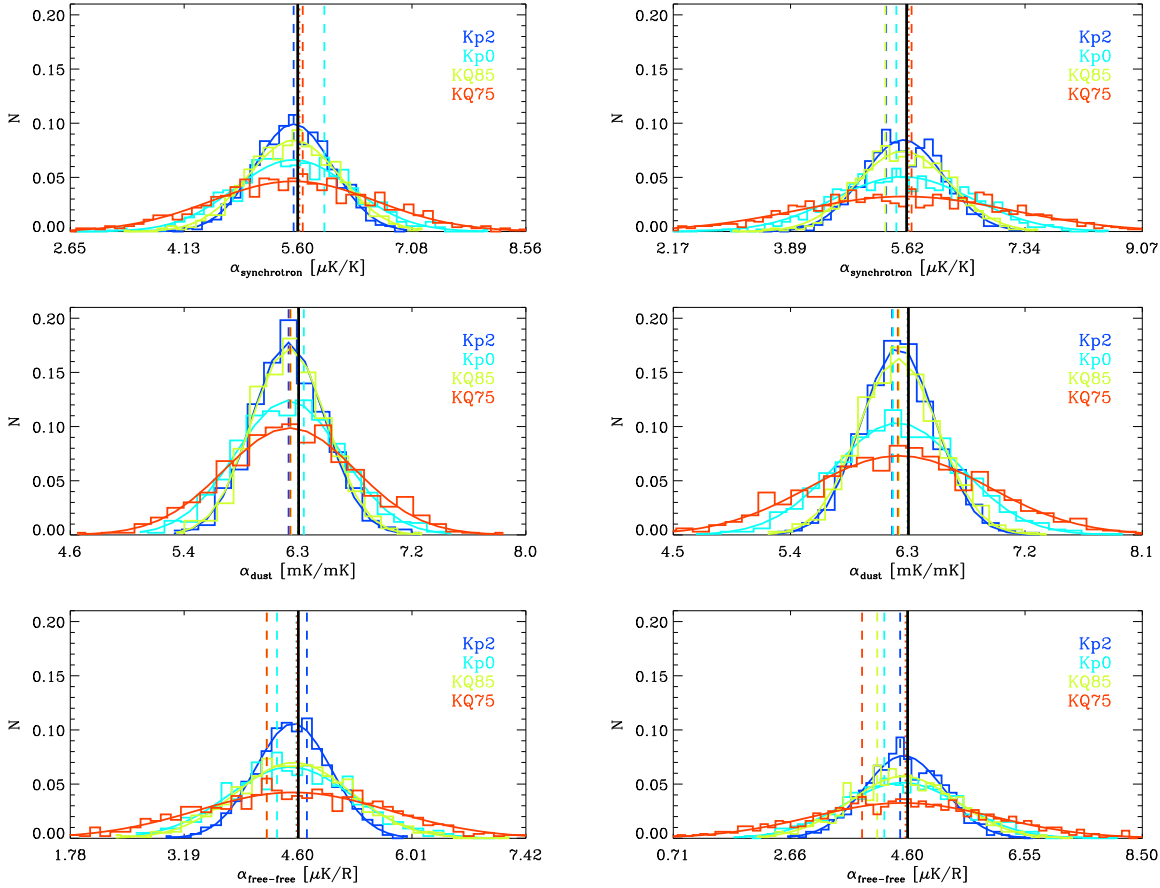


**Figure 1.** Histogram of the coupling coefficient distributions at K-band obtained from the simulations using the  $p$  (left) and  $g$  (right) functions and all the masks. Different color are associated to different masks in order to compare the results: blue for  $Kp2$ , cyan for  $Kp0$ , green for  $KQ85$  and red for  $KQ75$ . The dotted and dashed line show respectively the mean and the mode of the distributions, to be compared with the expected values (black line). For all the Galactic components except the dust emission, there is a strong dependence of the distribution width on the extension of the plane cut. This is particularly visible for the free-free emission where the scaling factors obtained with the  $KQ75$  mask are characterized by a very flat distribution.

nature of the integrated emission is complex, they should generally be excluded from analysis. Indeed the *WMAP* science team itself has proposed two new different masks than the previously used  $Kp2$  and  $Kp0$  cuts. They refer to the new masks as  $KQ85$  and  $KQ75$  since they are produced from the maps at the K and Q band and they exclude respectively 15% and 25% of the sky (Hinshaw et al. 2009). We employed all 4 masks together with a mask for the point sources, without any modification of the angular resolution. However, in the latter part of the paper we also experiment with a full-sky analysis as shown in section 9.

#### 4 MONTE CARLO SIMULATIONS

Monte Carlo simulations are used in this context for several reasons. First, they provide useful criteria and figures-of-merit that aid the selection of the non-linear function ( $p$ ,  $g$  or  $t$ ) used by the FASTICA algorithm to implement the component separation. Second, they provide a method to evaluate the level of correlation with and among the foregrounds. Finally we used these simulations to compute the uncertainties for the scaling factors presented in later sections of the paper.

We find that essentially all of the previous results from the 3-year analysis are confirmed. The reconstruction of the input coefficients is satisfactory for both the  $p$  and  $g$  functions, which provide similar results. Indeed, the distribution of the coefficients is a symmetric Gaussian function in both cases: the mean value is very close to the expected one and the mode differs only slightly. However, the  $g$  function shows generally a broader distribution compared to that for  $p$ , most likely as a consequence of the fact that they are sensitive to different statistical features of the spatial distribution of the sky radiation.

For the same reason the  $t$ -function remains inappropriate for template fitting: the statistical distributions of the returned coupling coefficients are asymmetric and highly biased with respect to the input values.

The distribution of the scaling factors generally depends on the mask used in the analysis (see figure 1): the more extensive the cut is, the larger is the dispersion of the values around the mean. It is particularly evident for the free-free emission where the  $KQ75$  mask is associated with the largest distribution, though it is still symmetric and not biased. We also find that the anti-correlation between the synchrotron and dust coefficients decreases for larger masks, as is the case for the correlation between the K-Ka template and the free-free.

The results from the simple  $\chi^2$  analysis indicate that the uncertainties for the synchrotron component are smaller than found using the FASTICA method, while they are larger for the other components. This method dependent cross-talk likely reflects the different statistical measures of the data employed by the FASTICA and  $\chi^2$  analyses.

## 5 COUPLING COEFFICIENTS BETWEEN DATA AND TEMPLATES

As noted above, the FASTICA component separation allows us to compute coupling coefficients between the data at each frequency of observation, and the three templates of the Galactic foreground components. We calculated these values using the  $p$  and the  $g$  non-linear functions and the four masks provided by the WMAP science team. Then, we compared the results with those from the simple  $\chi^2$  analysis. In table 1 and 2, we report the results obtained with two different sets of templates, where either the Haslam or the K-Ka map was used as synchrotron model. In the same tables, we show also the results from Bennett et al. (2003), Hinshaw et al. (2007) and Gold et al. (2009): these values are the WMAP results respectively for the 1-, 3- and 5-year foreground analysis corrections, with the  $Kp2$  or  $KQ85$  masks. In all three cases, some constraints were placed on the spectral behaviour of the components. In the first case the values were derived by fixing the synchrotron spectral index at a value of 2.7, and the free-free to 2.15 for frequencies above Q-band. In the latter cases, instead, they explicitly take into account the free-free signal present in the K-Ka template, and impose constraints on the free-free ( $\beta_{ff} = 2.14$ ) and thermal dust ( $\beta_d = 2$ ) spectral indices. However, we did not consider any constraints on the coefficients.

We note that the results obtained using the  $Kp2$  and  $Kp0$  masks are very consistent with those from our three-year analysis, with values varying at most by  $0.5\sigma$  with the previous ones. The frequency behavior is consistent with the theoretical expectations. The synchrotron and free-free emissions decrease with increasing frequency, whereas the dust coefficients are consistent with the superposition of an anomalous component with a falling contribution until approximately 61 GHz where a rising contribution from thermal emission is seen.

However, consideration of the results derived with the two new masks indicates that it is no longer possible to define a trend: a larger mask does not necessarily imply lower scaling factors, as was the case for the free-free coefficients obtained with the  $Kp2$  and the  $Kp0$  masks. On inspection of the results obtained with the Haslam map as synchrotron template, although the  $KQ75$  mask is the largest cut provided, we generally obtain values comparable to or higher than those returned using the  $Kp2$  and  $KQ85$  masks. It is certainly a confirmation of the fact that there exist spectral or physical variations of the foregrounds on the sky. These are particularly significant for the free-free emission and are presumably connected to specific regions near the Galactic plane, which are completely removed by the  $KQ75$  mask, but retained by the  $Kp2$  and  $KQ85$  cuts.

We studied the dependence of the analysis on the correction applied to the  $H\alpha$  map to correct for the dust absorption. The coupling coefficients show differences which are not very significant, but consistent with expectation, ie. as the absorption correction raises the  $H\alpha$  intensity, so the coefficients decrease. What is interesting then, is that the inconsistency between the values derived with the  $Kp0$  cut compared to the other masks still remains, implying that it is not easily associated with variations in the dust absorption. Thus it could be related to variations in the temperature of the ionized gas in the medium latitude regions. In fact, using the free-free coefficients we infer values of the electron temperature that change with the mask and that are generally lower than the expected value of 8000 K. This is true in particular for the  $Kp0$  mask.

The mask dependence is different for the K-Ka analysis. Each of the foreground components shows a specific trend with the cuts. In particular, the dust and free-free coefficients obtained with the  $KQ75$  mask are now lower than those with the  $Kp2$  and  $KQ85$  masks. However, this is not surprising, since the K-Ka map is a mix of different emissions. It has contributions from synchrotron and free-free, as well as from the anomalous component: none of which are present in the Haslam map (at high latitudes – there is a small contribution from free-free emission in the Galactic plane). Moreover, this can also be a possible explanation for the amplitudes of the dust coupling coefficients in the Q-band which are low compared to the Haslam case. Specifically, the anomalous component is now traced largely by the K-Ka template, rather than the dust. Indeed, this may also suggest that the thermal dust template is not morphologically identical to the anomalous dust emission, although well-correlated.

We have also used a simple  $\chi^2$  analysis as a standard method to be compared with FASTICA. Whereas with the WMAP 3-year data we considered only the results for the  $Kp2$  mask, here we extend the comparison to all of the sky coverages. This choice was motivated by the unusual dependence on the extension of the mask observed in our analysis. With the Haslam map as synchrotron template, the anomaly is confirmed by the  $\chi^2$  analysis. In fact the FASTICA numbers are generally in good

	synchrotron		dust		free-free	
	$Kp2$	$Kp0$	$Kp2$	$Kp0$	$Kp2$	$Kp0$
FASTICA - function $p$						
$K$	$6.20 \pm 0.49$	$5.47 \pm 0.75$	$5.88 \pm 0.29$	$4.96 \pm 0.40$	$8.57 \pm 0.47$	$6.66 \pm 0.75$
$Ka$	$1.91 \pm 0.49$	$1.70 \pm 0.74$	$2.04 \pm 0.28$	$1.29 \pm 0.38$	$4.35 \pm 0.46$	$2.74 \pm 0.74$
$Q$	$0.96 \pm 0.48$	$0.87 \pm 0.74$	$1.09 \pm 0.28$	$0.44 \pm 0.37$	$2.91 \pm 0.46$	$1.34 \pm 0.73$
$V$	$0.26 \pm 0.46$	$0.24 \pm 0.70$	$0.61 \pm 0.26$	$0.05 \pm 0.35$	$1.34 \pm 0.43$	$-0.07 \pm 0.70$
$W$	$0.06 \pm 0.40$	$0.07 \pm 0.61$	$0.97 \pm 0.23$	$0.46 \pm 0.31$	$0.64 \pm 0.38$	$-0.52 \pm 0.61$
FASTICA - function $g$						
$K$	$6.42 \pm 0.58$	$5.63 \pm 0.95$	$6.14 \pm 0.30$	$5.76 \pm 0.48$	$8.48 \pm 0.65$	$6.52 \pm 0.97$
$Ka$	$2.04 \pm 0.56$	$1.91 \pm 0.94$	$2.10 \pm 0.29$	$1.68 \pm 0.47$	$4.26 \pm 0.64$	$2.80 \pm 0.95$
$Q$	$1.10 \pm 0.56$	$1.12 \pm 0.92$	$1.11 \pm 0.29$	$0.71 \pm 0.47$	$2.79 \pm 0.63$	$1.45 \pm 0.94$
$V$	$0.40 \pm 0.53$	$0.54 \pm 0.87$	$0.60 \pm 0.27$	$0.24 \pm 0.44$	$1.21 \pm 0.60$	$0.03 \pm 0.89$
$W$	$0.19 \pm 0.46$	$0.33 \pm 0.77$	$0.95 \pm 0.24$	$0.61 \pm 0.39$	$0.56 \pm 0.53$	$-0.41 \pm 0.78$
$\chi^2$ analysis						
$K$	$5.98 \pm 0.42$	$5.42 \pm 0.57$	$6.44 \pm 0.31$	$6.34 \pm 0.55$	$7.93 \pm 0.74$	$5.68 \pm 1.20$
$Ka$	$1.84 \pm 0.42$	$1.62 \pm 0.56$	$2.26 \pm 0.30$	$2.12 \pm 0.54$	$3.77 \pm 0.73$	$2.11 \pm 1.18$
$Q$	$0.92 \pm 0.41$	$0.79 \pm 0.56$	$1.24 \pm 0.30$	$1.12 \pm 0.53$	$2.31 \pm 0.72$	$0.80 \pm 1.17$
$V$	$0.24 \pm 0.39$	$0.17 \pm 0.53$	$0.71 \pm 0.28$	$0.62 \pm 0.51$	$0.75 \pm 0.68$	$-0.59 \pm 1.11$
$W$	$0.04 \pm 0.34$	$-0.01 \pm 0.46$	$1.04 \pm 0.25$	$0.94 \pm 0.45$	$0.17 \pm 0.60$	$-0.95 \pm 0.97$
<b>Bennett et al. (constrained: <math>\beta_s = 2.7</math>; <math>\beta_{ff} = 2.15</math>)</b>						
$K$	–	–	–	–	–	–
$Ka$	–	–	–	–	–	–
$Q$	1.01	–	1.04	–	(1.92)	–
$V$	0.34	–	0.62	–	(0.82)	–
$W$	0.11	–	0.87	–	(0.32)	–
	$KQ85$	$KQ75$	$KQ85$	$KQ75$	$KQ85$	$KQ75$
FASTICA - function $p$						
$K$	$6.57 \pm 0.58$	$6.05 \pm 1.09$	$5.62 \pm 0.29$	$4.78 \pm 0.51$	$8.32 \pm 0.72$	$8.14 \pm 1.15$
$Ka$	$2.28 \pm 0.57$	$2.58 \pm 1.08$	$2.04 \pm 0.28$	$1.66 \pm 0.51$	$4.47 \pm 0.71$	$4.51 \pm 1.14$
$Q$	$1.36 \pm 0.56$	$1.85 \pm 1.06$	$1.17 \pm 0.28$	$0.95 \pm 0.50$	$3.12 \pm 0.70$	$3.23 \pm 1.12$
$V$	$0.64 \pm 0.54$	$1.29 \pm 1.01$	$0.76 \pm 0.27$	$0.67 \pm 0.47$	$1.66 \pm 0.67$	$1.92 \pm 1.06$
$W$	$0.38 \pm 0.47$	$0.94 \pm 0.89$	$1.11 \pm 0.24$	$1.01 \pm 0.42$	$0.95 \pm 0.59$	$1.16 \pm 0.93$
FASTICA - function $g$						
$K$	$6.45 \pm 0.65$	$6.34 \pm 1.47$	$6.00 \pm 0.31$	$6.37 \pm 0.69$	$7.72 \pm 0.86$	$6.18 \pm 1.56$
$Ka$	$2.25 \pm 0.64$	$3.02 \pm 1.45$	$2.09 \pm 0.31$	$2.39 \pm 0.68$	$3.85 \pm 0.85$	$2.93 \pm 1.53$
$Q$	$1.33 \pm 0.63$	$2.31 \pm 1.43$	$1.16 \pm 0.30$	$1.47 \pm 0.67$	$2.49 \pm 0.84$	$1.73 \pm 1.51$
$V$	$0.65 \pm 0.60$	$1.76 \pm 1.35$	$0.69 \pm 0.29$	$1.05 \pm 0.63$	$1.03 \pm 0.80$	$0.53 \pm 1.44$
$W$	$0.40 \pm 0.53$	$1.34 \pm 1.19$	$1.03 \pm 0.25$	$1.29 \pm 0.56$	$0.44 \pm 0.70$	$-0.01 \pm 1.26$
$\chi^2$ analysis						
$K$	$5.91 \pm 0.46$	$5.33 \pm 0.70$	$6.36 \pm 0.34$	$6.67 \pm 0.75$	$7.06 \pm 1.00$	$4.99 \pm 1.85$
$Ka$	$1.86 \pm 0.45$	$1.63 \pm 0.69$	$2.29 \pm 0.33$	$2.47 \pm 0.73$	$3.25 \pm 0.99$	$1.88 \pm 1.82$
$Q$	$0.97 \pm 0.45$	$0.83 \pm 0.68$	$1.32 \pm 0.33$	$1.49 \pm 0.72$	$1.90 \pm 0.98$	$0.73 \pm 1.79$
$V$	$0.30 \pm 0.42$	$0.22 \pm 0.64$	$0.82 \pm 0.31$	$1.01 \pm 0.69$	$0.45 \pm 0.93$	$-0.48 \pm 1.70$
$W$	$0.09 \pm 0.37$	$0.03 \pm 0.57$	$1.13 \pm 0.28$	$1.27 \pm 0.60$	$-0.06 \pm 0.81$	$-0.88 \pm 1.50$

**Table 1.** Values of the coupling coefficients in antenna temperature units determined between the 5-year *WMAP* data and three foreground emission templates, at  $1^\circ$  resolution. The Haslam 408 MHz map is adopted as the synchrotron template. The FASTICA analysis is performed using the two non-linear functions  $p$  and  $g$  and four masks of the Galactic plane. The corresponding results for a simple  $\chi^2$  analysis are provided for comparison. In addition, we provide the values from the *WMAP* 1-year (Bennett et al. 2003) fits to the Q, V and W-bands performed with constraints imposed on the synchrotron and free-free spectral indices. The units are  $\mu\text{K}/\text{K}$  for synchrotron,  $\text{mK}/\text{mK}$  for dust and  $\mu\text{K}/\text{R}$  for free-free emission respectively.

	synchrotron		dust		free-free	
	$Kp2$	$Kp0$	$Kp2$	$Kp0$	$Kp2$	$Kp0$
FASTICA - function $p$						
$Q$	$0.18 \pm 0.08$	$0.15 \pm 0.12$	$0.40 \pm 0.40$	$0.12 \pm 0.58$	$2.16 \pm 0.60$	$0.67 \pm 0.89$
$V$	$-0.00 \pm 0.08$	$-0.03 \pm 0.12$	$0.63 \pm 0.38$	$0.38 \pm 0.55$	$1.33 \pm 0.57$	$-0.05 \pm 0.84$
$W$	$-0.05 \pm 0.07$	$-0.07 \pm 0.10$	$1.16 \pm 0.34$	$0.92 \pm 0.48$	$0.82 \pm 0.50$	$-0.32 \pm 0.74$
FASTICA - function $g$						
$Q$	$0.25 \pm 0.10$	$0.16 \pm 0.17$	$0.15 \pm 0.47$	$0.13 \pm 0.80$	$1.76 \pm 0.79$	$0.82 \pm 1.17$
$V$	$0.06 \pm 0.09$	$-0.02 \pm 0.16$	$0.41 \pm 0.45$	$0.41 \pm 0.76$	$0.94 \pm 0.75$	$0.05 \pm 1.11$
$W$	$0.01 \pm 0.08$	$-0.06 \pm 0.14$	$0.96 \pm 0.40$	$0.93 \pm 0.67$	$0.50 \pm 0.66$	$-0.24 \pm 0.98$
$\chi^2$ analysis						
$Q$	$0.22 \pm 0.09$	$0.20 \pm 0.12$	$0.37 \pm 0.41$	$0.33 \pm 0.68$	$1.43 \pm 0.85$	$0.11 \pm 1.21$
$V$	$0.03 \pm 0.08$	$0.01 \pm 0.11$	$0.59 \pm 0.39$	$0.53 \pm 0.64$	$0.76 \pm 0.81$	$-0.47 \pm 1.15$
$W$	$-0.01 \pm 0.07$	$-0.02 \pm 0.10$	$1.10 \pm 0.34$	$1.04 \pm 0.56$	$0.29 \pm 0.71$	$-0.81 \pm 1.01$
Hinshaw et al. (constrained: $\beta_{ff} = 2.14$ ; $\beta_s = 2$ )						
$Q$	0.23		0.19		0.99	
$V$	0.05		0.41		0.63	
$W$	0.00		0.98		0.32	
	$KQ85$	$KQ75$	$KQ85$	$KQ75$	$KQ85$	$KQ75$
FASTICA - function $p$						
$Q$	$0.28 \pm 0.10$	$0.44 \pm 0.13$	$0.27 \pm 0.42$	$-0.29 \pm 0.66$	$2.03 \pm 0.84$	$1.54 \pm 1.16$
$V$	$0.10 \pm 0.09$	$0.25 \pm 0.13$	$0.51 \pm 0.40$	$0.03 \pm 0.62$	$1.25 \pm 0.79$	$0.89 \pm 1.09$
$W$	$0.04 \pm 0.08$	$0.15 \pm 0.11$	$1.08 \pm 0.35$	$0.66 \pm 0.55$	$0.78 \pm 0.70$	$0.48 \pm 0.96$
FASTICA - function $g$						
$Q$	$0.30 \pm 0.12$	$0.35 \pm 0.36$	$0.06 \pm 0.53$	$0.11 \pm 1.56$	$1.34 \pm 0.99$	$0.39 \pm 1.59$
$V$	$0.12 \pm 0.11$	$0.16 \pm 0.36$	$0.31 \pm 0.50$	$0.43 \pm 1.10$	$0.55 \pm 0.94$	$-0.24 \pm 1.51$
$W$	$0.06 \pm 0.10$	$0.07 \pm 0.31$	$0.87 \pm 0.44$	$1.04 \pm 0.97$	$0.19 \pm 0.83$	$-0.45 \pm 1.33$
$\chi^2$ analysis						
$Q$	$0.23 \pm 0.10$	$0.21 \pm 0.14$	$0.43 \pm 0.44$	$0.66 \pm 0.90$	$1.05 \pm 1.06$	$0.07 \pm 1.73$
$V$	$0.04 \pm 0.09$	$0.03 \pm 0.13$	$0.65 \pm 0.42$	$0.84 \pm 0.86$	$0.46 \pm 1.00$	$-0.35 \pm 1.64$
$W$	$-0.00 \pm 0.08$	$-0.01 \pm 0.11$	$1.14 \pm 0.37$	$1.29 \pm 0.75$	$0.00 \pm 0.88$	$-0.79 \pm 1.44$
Gold et al. (constrained: $\beta_{ff} = 2.14$ ; $\beta_s = 2$ )						
$Q$	0.23		0.19		0.95	
$V$	0.05		0.43		0.60	
$W$	0.00		1.01		0.32	

**Table 2.** Values of the coupling coefficients in antenna temperature units determined between the 5-year WMAP data in the Q, V and W band and three foreground emission templates, at  $1^\circ$  resolution. The K-Ka map is adopted as the synchrotron template. The FASTICA analysis is performed using the two non-linear functions  $p$  and  $g$  and four masks of the Galactic plane. The corresponding results for a simple  $\chi^2$  analysis are provided for comparison. In addition, we provide where appropriate the values from the WMAP 3-year (Hinshaw et al. 2007) and 5-year (Gold et al. 2009) fits to the Q,V and W-bands performed with constraints imposed on the synchrotron and free-free spectral indices. The units are mK/mK for synchrotron, mK/mK for dust and  $\mu\text{K/R}$  for free-free emission respectively.

statistical agreement with the  $\chi^2$  results, even though the synchrotron and dust amplitudes are systematically lower (higher) for the  $\chi^2$  method. However, this in general reflects the weak cross-talk seen between the fitted amplitudes. Alternately, when the K-Ka map is adopted instead, the  $\chi^2$  coupling coefficients of the synchrotron and dust emission are stable with respect to the mask used. Conversely, the free-free coefficients are found to be strongly dependent on the cut. Moreover, the values obtained with the  $Kp0$  and  $KQ75$  masks are consistent with zero. Nevertheless, all the coefficients are consistent with the FASTICA results.

Finally, we compared our results with those obtained by Bennett et al. (2003), Hinshaw et al. (2007) and Gold et al. (2009) with constrained fits. The values are comparable for the synchrotron and dust emissions, with both the synchrotron templates. The free-free values, however, are notably different in all the cases, in part due to the fact that they corrected

	Synchrotron		Anomalous Component		Free-Free	
FASTICA – function p						
	<i>Kp2</i>	<i>Kp0</i>	<i>Kp2</i>	<i>Kp0</i>	<i>Kp2</i>	<i>Kp0</i>
$\beta$	$3.25^{+1.18}_{-0.49}$	$3.21^{+1.23}_{-0.54}$	$3.32^{+0.48}_{-0.26}$	$4.72^{+0.31}_{-0.36}$	$1.88^{+0.62}_{-0.50}$	$2.89^{+1.28}_{-0.38}$
$A_{norm}$	$6.20 \pm 0.47$	$5.46 \pm 0.72$	$5.79 \pm 0.20$	$4.87 \pm 0.28$	$8.57 \pm 0.44$	$6.76 \pm 0.69$
	<i>KQ85</i>	<i>KQ75</i>	<i>KQ85</i>	<i>KQ75</i>	<i>KQ85</i>	<i>KQ75</i>
$\beta$	$2.70^{+1.11}_{-0.46}$	$1.80^{+0.90}_{-0.75}$	$3.09^{+0.39}_{-0.33}$	$3.29^{+0.25}_{-0.50}$	$1.65^{+0.23}_{-0.58}$	$1.51^{+0.41}_{-0.41}$
$A_{norm}$	$6.52 \pm 0.56$	$5.84 \pm 1.02$	$5.52 \pm 0.20$	$4.67 \pm 0.37$	$8.27 \pm 0.66$	$8.05 \pm 0.91$
FASTICA – function g						
	<i>Kp2</i>	<i>Kp0</i>	<i>Kp2</i>	<i>Kp0</i>	<i>Kp2</i>	<i>Kp0</i>
$\beta$	$3.06^{+1.35}_{-0.56}$	$2.76^{+1.07}_{-0.75}$	$3.35^{+0.42}_{-0.31}$	$4.09^{+0.54}_{-0.38}$	$1.94^{+0.31}_{-0.52}$	$2.74^{+1.28}_{-0.24}$
$A_{norm}$	$6.41 \pm 0.55$	$5.59 \pm 0.90$	$6.05 \pm 0.21$	$5.68 \pm 0.35$	$8.50 \pm 0.60$	$6.62 \pm 1.09$
	<i>KQ85</i>	<i>KQ75</i>	<i>KQ85</i>	<i>KQ75</i>	<i>KQ85</i>	<i>KQ75</i>
$\beta$	$2.69^{+1.11}_{-0.46}$	$1.41^{+0.90}_{-0.75}$	$3.23^{+0.45}_{-0.28}$	$2.79^{+0.71}_{-0.16}$	$1.99^{+0.30}_{-0.50}$	$2.28^{+0.72}_{-0.13}$
$A_{norm}$	$6.40 \pm 0.63$	$6.00 \pm 1.34$	$5.90 \pm 0.22$	$6.23 \pm 0.51$	$7.75 \pm 0.81$	$6.25 \pm 1.03$
$\chi^2$						
	<i>Kp2</i>	<i>Kp0</i>	<i>Kp2</i>	<i>Kp0</i>	<i>Kp2</i>	<i>Kp0</i>
$\beta$	$3.26^{+1.39}_{-0.48}$	$3.37^{+1.23}_{-0.54}$	$3.20^{+0.36}_{-0.38}$	$3.39^{+0.34}_{-0.32}$	$2.20^{+0.66}_{-0.55}$	$3.44^{+0.72}_{-0.24}$
$A_{norm}$	$5.98 \pm 0.41$	$5.43 \pm 0.54$	$6.34 \pm 0.22$	$6.25 \pm 0.40$	$7.99 \pm 0.68$	$5.78 \pm 1.01$
	<i>KQ85</i>	<i>KQ75</i>	<i>KQ85</i>	<i>KQ75</i>	<i>KQ85</i>	<i>KQ75</i>
$\beta$	$3.14^{+1.11}_{-0.46}$	$3.26^{+0.86}_{-0.86}$	$3.06^{+0.30}_{-0.45}$	$2.86^{+0.71}_{-0.16}$	$2.38^{+0.30}_{-0.50}$	$-3.39^{+0.41}_{-0.41}$
$A_{norm}$	$5.90 \pm 0.44$	$5.33 \pm 0.61$	$6.26 \pm 0.24$	$6.55 \pm 0.55$	$7.14 \pm 0.89$	$5.07 \pm 1.36$

**Table 3.** Spectral index  $\beta$  and normalisation factor  $A_{norm}$  obtained fitting values of the coupling coefficients for synchrotron (as traced by the Haslam template), the anomalous component of dust and free-free emission, with different masks. The normalization factor  $A_{norm}$  has units equal to mK/mK for synchrotron, mK/mK for dust and  $\mu\text{K}/\text{R}$  for free-free emission respectively.

the  $\text{H}\alpha$  map for dust absorption. However, even if we repeat our analysis using the *WMAP* value for the dust absorption correction, the coefficients remain larger than *WMAP* derive. Therefore, it cannot be the only explanation for the difference.

### 5.1 Spectral index of foreground emissions.

We parameterise the spectral behavior of the synchrotron emission (as traced by the Haslam template), the anomalous dust component, and free-free emission with particular emphasis on the latter. The *WMAP* frequency range does not allow a detailed study of the spectral behaviour of the thermal component of dust. We fitted the coefficients of each component with a power law model of the form  $A_{norm}(\nu/\nu_0)^{-\beta}$ .  $A_{norm}$  is the amplitude of the emission of a specific physical component at the reference frequency  $\nu_0$ , which we take as the K-band (23 GHz). In the case of the anomalous component, in order to isolate its contribution we recomputed the coefficients from the sky maps after correcting them for a thermal dust contribution assuming the FDS8 dust model. This assumption is consistent with the W-band correlation results in table 1.

Since, the *Kp2* and *Kp0* results do not show any significant difference with respect to those computed with the *WMAP* 3-year data, we do not expect the spectral index to change and this is indeed seen to be the case in table 3. For the synchrotron emission, using the *Kp2* mask the spectral index is steeper than  $\beta_s = 3.0$ , even though still consistent, while it is flatter for the *Kp0* mask, particularly when using the *g*-function. The values of the spectral index  $\beta_a$  of the anomalous dust component are larger than 3 especially if the *Kp0* mask is adopted. Therefore, they are steeper than the value of 2.85 obtained by Davies et al. (2006), although higher values of the spectral index are expected if we consider regions of the sky at mid- to high-latitude. In fact, Davies et al. (2006) have also noted spectral indices as steep as 3.8 in several dust dominated regions.

However, the values obtained with the new masks highlight some unexpected physical properties of the foreground components. In fact, with the *KQ85* and *KQ75* masks, the synchrotron and anomalous dust spectral indices are flatter than those derived from the older *Kp2* and *Kp0* masks, and in some cases considerably so. Indeed, whilst all values are consistent within the errors (derived from simulations), we are unable to explain these differences given that the new masks can be



Free-Free				
FASTICA – function p				
	<i>Kp2</i>	<i>Kp0</i>	<i>KQ85</i>	<i>KQ75</i>
$F_0$	$8.21 \pm 0.63$	$7.73 \pm 1.01$	$7.52 \pm 0.97$	$7.05 \pm 1.55$
$D_0$	$0.05 \pm 0.10$	$0.05 \pm 0.16$	$0.05 \pm 0.15$	$0.04 \pm 0.24$
$C_0$	$0.31 \pm 0.38$	$-1.13 \pm 0.61$	$0.75 \pm 0.59$	$1.07 \pm 0.94$
FASTICA – function g				
	<i>Kp2</i>	<i>Kp0</i>	<i>KQ85</i>	<i>KQ75</i>
$F_0$	$8.24 \pm 0.87$	$7.43 \pm 1.30$	$7.59 \pm 1.16$	$6.49 \pm 2.09$
$D_0$	$0.05 \pm 0.13$	$0.06 \pm 0.20$	$0.05 \pm 0.18$	$0.06 \pm 0.32$
$C_0$	$0.19 \pm 0.53$	$-0.99 \pm 0.79$	$0.08 \pm 0.70$	$-0.37 \pm 1.26$
$\chi^2$				
	<i>Kp2</i>	<i>Kp0</i>	<i>KQ85</i>	<i>KQ75</i>
$F_0$	$8.16 \pm 1.00$	$7.24 \pm 1.62$	$7.54 \pm 1.35$	$6.37 \pm 2.48$
$D_0$	$0.06 \pm 0.15$	$0.07 \pm 0.25$	$0.06 \pm 0.21$	$0.07 \pm 0.38$
$C_0$	$-0.29 \pm 0.60$	$-1.65 \pm 0.98$	$-0.54 \pm 0.82$	$-1.47 \pm 1.50$

**Table 4.** Values of the parameters obtained fitting the free-free coupling coefficients with the model proposed by Dobler et al. (2008b) (see equation 1). The coefficients are those derived using both FASTICA and the  $\chi^2$  analysis.  $C_0$  and  $D_0$  are consistent with zero, the later result demonstrating that we do not find any evidence of a spinning dust admixture with the free-free emission. The units of the parameters are kJy/sr/R.

considered as small modifications to the older ones. The major difference relates to the omission now of various features associated with the free-free emission. That such apparently small changes can affect the FASTICA analysis to such an extent might be considered problematic, although it may ultimately be telling us something about the properties of the foregrounds close to the mask boundaries.

With regards to the free-free emission, the previous analysis in Bottino et al. (2008) found suggestions of anomalous behaviour that remain to be explained. Our fits for all of the sky coverages are statistically consistent with the expected scaling for free-free emission with frequency,  $\beta_{ff} = 2.14$ . Nonetheless, depending on the extension of the cut the spectral behaviour of the coefficients show different trends, as already pointed out in the earlier work. Comparing the spectral behaviour recovered with the different Galactic cuts, the index is always flatter than the canonical value of 2.14 except with the *Kp0* mask which is steeper. Previously, we had interpreted this result as the consequence of different properties of the free-free emission close to the plane (perhaps a mixture of regions with different electron temperatures), the presence of spinning dust in the WIM, or simply cross-talk between different physical components that confuses the spectral analysis.

Here, we consider the second option in more detail by adopting a model proposed by Dobler et al. (2008b). For consistency with their analysis, we consider the template fit coefficients after conversion into intensity units. Practically, the coefficients relative to the H $\alpha$  template are described as a mix of free-free emission ( $F_0$ ) and radiation from the WIM ( $D_0$ ) that together generate the spectral bump that Dobler et al. (2008b) observe. The final term ( $C_0$ ) with a CMB-like spectrum is a consequence of the initial subtraction of an estimate of the CMB sky before undertaking the template fitting. Thus the derived free-free coefficients are parameterised by the following relation:

$$I_{mod} = F_0 \left( \frac{\nu}{23GHz} \right)^{-0.15} + D_0(DL98, v_{peak} = 40GHz) + C_0 \left( \frac{\nu}{23GHz} \right)^2 a(\nu) \quad (1)$$

where DL98 is the WIM model of spinning dust due to Draine et al. (1998b), but shifted in order to have the maximum emission at 40GHz, and where  $a(\nu)$  represents the conversion factor from thermodynamic to antenna temperature at a given frequency. In fact Dobler et al. (2008b) utilise several variants of the CMB sky estimated by internal linear combination (ILC) methods. Since an ILC map will necessarily contain foreground residuals, the ILC-corrected data contain modified amounts of the expected foreground levels, and the  $C_0$  term effectively attempts to correct for this bias. Since we did not pre-process the data in the same way, we do not formally need to include this term in the analysis, but do so in the expectation that the coefficient  $C_0$  will be consistent with zero. This is, in fact, the case, and more importantly, as shown in table 4, the  $D_0$  dust coefficient is also consistent with zero – we do not find any evidence of a spinning dust admixture with the free-free emission. Interestingly, the simple  $\chi^2$  analysis yields a spectral index that is very consistent with theoretical expectations ( $\sim 0.14$ ), especially with the *Kp2* and *KQ85* masks.

As noted before, the different treatment of the CMB component in the derivation of the coefficients, together with the

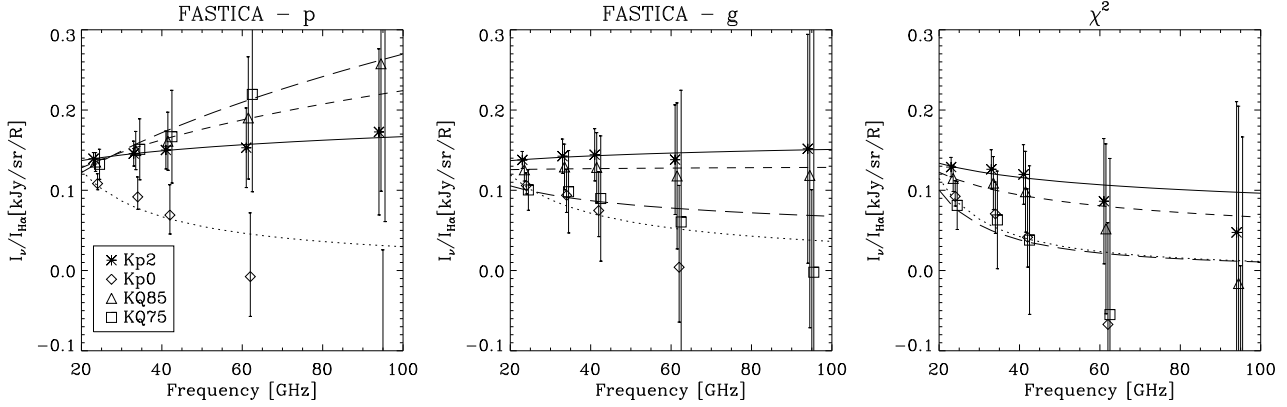


**Figure 2.** The coupling coefficients in intensity units (kJy/sr/R) for free-free emission as traced by the  $H\alpha$  template. We show the results from the FASTICA  $p$  function analysis are in the leftmost plot, from the  $g$  function in the middle plot, and the values from the  $\chi^2$  analysis are shown on the right. Asterisks represent the derived amplitudes for the  $Kp2$  sky coverage, diamonds are for  $Kp0$ , the triangles for  $KQ85$  and the squares for  $KQ75$ . Best-fit curves are also shown. The FASTICA  $p$  results show an anomalous rising spectrum for the free-free emissivity with all the masks but the  $Kp0$ , whereas with the  $g$  function and the  $\chi^2$  analysis the results are more consistent with expectations. The  $Kp0$  mask shows consistently a steeper spectrum than expected. The  $\chi^2$  results are consistent with the expectations for free-free emission.

different fitting methodologies, seem to play important roles in attempting a reasonable interpretation of the results and a connection to what has been found by other authors. Indeed, cross-talk between the CMB and foreground emission – the so-called ‘cosmic covariance’ of Chiang et al. (2009) – can likely both flatten and steepen the determined spectrum in some cases, and Dobler et al. (2008b) have proposed that this effect makes it mandatory to subtract a CMB estimate before attempting any template fitting. In fact, we have observed such spectral changes in a set of simulations in which the foregrounds are described with idealised spectra (ie.  $\beta_s = 3.1$ ,  $\beta_{ff} = 2.15$ ,  $\beta_d = 1.7$ , and a contribution from an  $H\alpha$  correlated WIM spinning dust component is either included or otherwise). However, the typical behaviour is such that the latter component is not detected erroneously when it is absent, and is detected when present. We do not then find a likely explanation of the inconsistency of our results with Dobler et al. (2008b) given our unbiased recovery of the input coefficients.

## 6 EVALUATION OF THE *WMAP* SKY MAPS AFTER FOREGROUND CLEANING

Computing the coupling coefficients between the *WMAP* data and the foreground templates is useful both to study the spectral properties of the foregrounds and to allow the data to be cleaned for subsequent cosmological analysis. In our approach, we apply the FASTICA method to large sky areas, thus effectively assuming that each foreground has a single spectral index over the region of interest. In reality, this is incorrect, and we therefore expect that the cleaned data will contain residual foreground contamination, as a consequence both of this assumption, and the related one that the templates do indeed provide an adequate representation of the foreground morphology at microwave wavelengths. The study of such residuals is then itself important in order to gain new physical insight, and to evaluate their impact on the statistical properties of the cleaned CMB maps. We have followed this approach in the 3-year analysis of Bottino et al. (2008).

In this paper, we wish to experiment further with the implementation of the cleaning approach applied to the data. To that end, we should recall that the coefficients are derived by maximising an approximation to the neg-entropy over the sky fraction of interest. Such a non-linear function could be dominated by one or two regions, that are either bright or have complex morphologies, thus the derived coefficients would be sub-optimal elsewhere. Indeed, one might speculate that such regions would occur close to the Galactic plane. Conversely, with a mask that only allows high latitude regions to be analysed where the spectral variations may be smaller, the coefficients may allow a relatively efficient cleaning of the data and small amounts of residuals. An interesting question then becomes by how much low latitude residuals would increase if the high latitude coefficients are applied. We therefore determine the template coefficients as a function of mask, apply the corresponding corrections to the multi-frequency data, and then inspect the corrected maps. In section 7 we then investigate the related impact on an iterative cleaning approach. We show only the results based on the  $p$ -function analysis, since there is little visual difference relative to the  $g$ -function.

Figures 3 and 4 show the results for the Q-, V- and W-band data. We show two maps at each frequency - each map corresponds to the data as cleaned following the template analysis with the specified mask, but both the masked and full-sky are plotted. Showing the latter can help to reveal spectral mismatches between the emission in the masked region and the

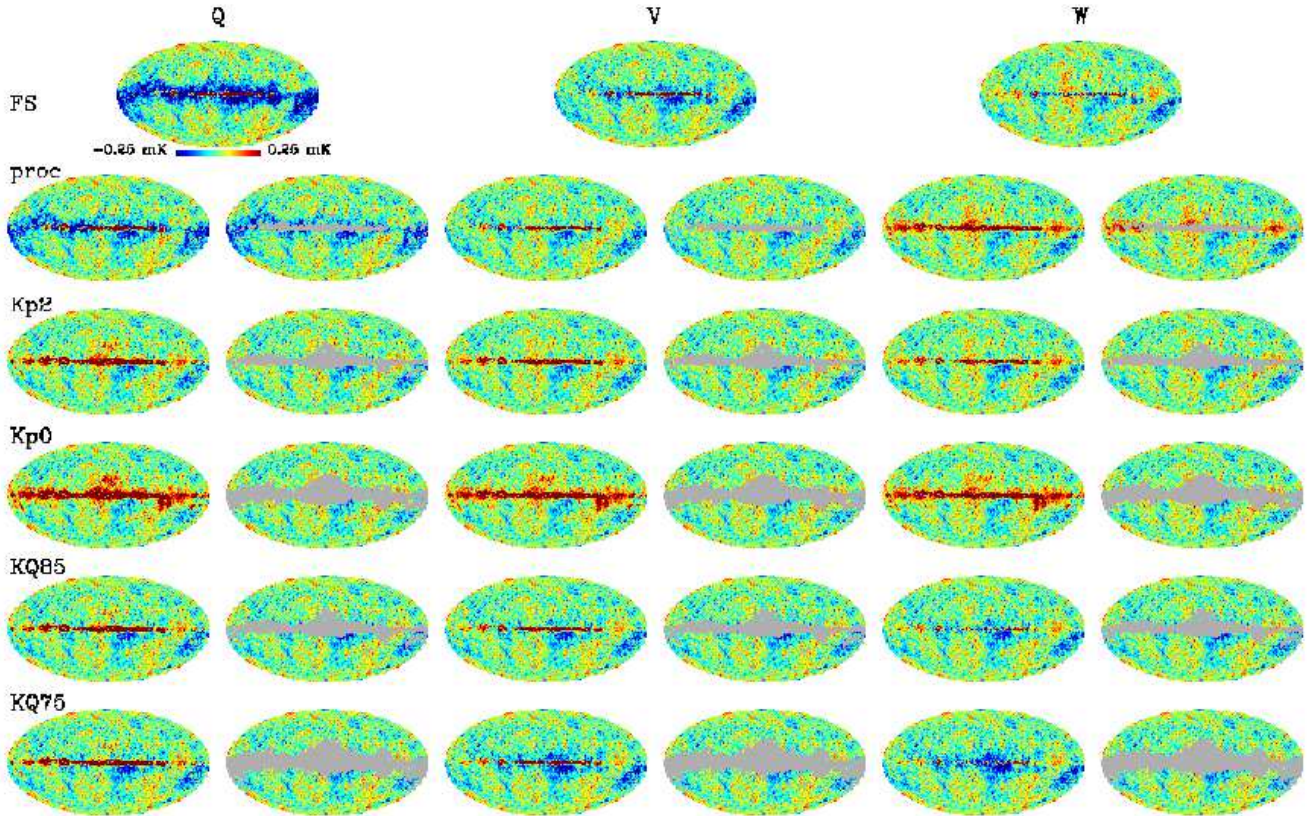


**Figure 3.** *WMAP* Q-, V- and W-band cleaned by subtracting foreground templates scaled by the coupling coefficients determined by FASTICA with the  $p$ -function. The maps are shown in a conventional mollweide projection in a Galactic frame-of-reference, with the north pole at the top of the image and the Galactic Center in the middle with longitude increasing to the left. The regions in grey correspond to the bright Galactic emission and point sources excised from the analysis by the masks. Each row corresponds to maps cleaned by coefficients derived from an analysis using one of 6 masks – FS (full sky, although the point source mask is still employed), proc (the processing mask), Kp2, Kp0, KQ85 and KQ75. The columns are divided into three pairs, each pair corresponding to one of the three frequencies considered as indicated. The left-hand plot in the pair is the full-sky map cleaned using the coefficients derived when applying the indicated mask, the right-hand plot then shows the cleaned map with the appropriate mask applied. The structure visible on the full-sky that falls within the analysis mask indicates the effect of spectral mismatch between the low- and high-latitude sky. Clearly, the first row can only show one map since the two cases coincide for a full-sky analysis. Here, the adopted synchrotron template is the Haslam map.

high-latitude area used for the analysis. The exception is the full-sky (FS) analysis where only the point-sources are masked in the analysis. It is clear that there is a complex pattern of behaviour as a function of mask, and some dependence on the template used to trace the synchrotron emission. However, with either the Haslam or K-Ka templates, it is apparent that in general, the thinner the applied mask, the higher the level of residual contamination. It should also be noted that in most cases the  $Kp0$  results seem anomalous and larger residuals are observed. When the Haslam template is used as the synchrotron tracer (figure 3) the Q-band residuals towards the plane are the largest in amplitude, with the V- and W-band comparable. However, the residuals corresponding to fits performed on either the full-sky or using the processing mask are largely negative for the Q-band - there is an over-correction for foregrounds towards the Galactic plane. Interestingly, the low latitude residuals at V- and W-band for the full-sky analysis are relatively small and positive and confined to a very thin disk (a similar structure is seen at Q-band though embedded in the larger region of over-subtracted foregrounds). However, there appear to be more structures at higher latitudes than when more extensive masks are applied. Not surprisingly, the foreground coefficients are driven by the high amplitude Galactic plane signal, but are then sub-optimal for the high-latitude corrections. For the masks commonly applied for *WMAP* analysis, the cleaned maps at high latitude look very consistent, and the low-latitude residuals tend to be smallest for W-band. As noted above, the  $Kp0$  results are a curiosity and the level of residuals seems unexpectedly to be higher than for either the  $Kp2$ ,  $KQ85$  or  $KQ75$  masks, the latter case perhaps indicating some connection to the bright free-free regions that are masked therein. This argument may well be supported by the clear excess towards the Gum nebula. However, with the non-linear analysis performed by FASTICA it is difficult to be too precise about the origin of this behaviour. For the K-Ka template, the low-latitude residuals are generally positive except for the

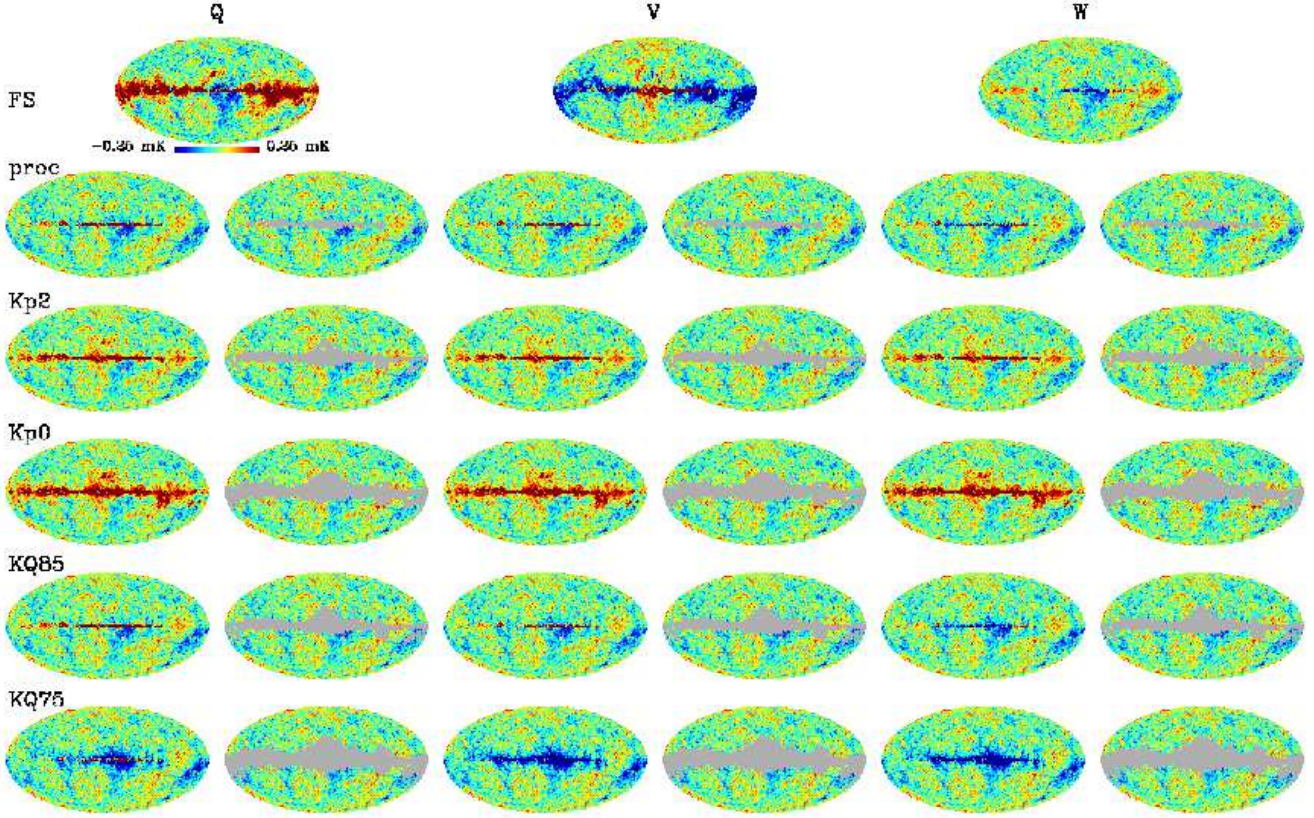


**Figure 4.** As the previous figure, but using the K-Ka template for tracing the low frequency foreground emission.

full-sky analysis where there is a complex mix of positive and negative structures at Q- and V-band, and for the *KQ75* mask where the residuals are predominantly negative. The results seem to suggest an improved cleaning of the data, particularly at intermediate latitudes. It is again reassuring to note that, in all cases, the dominant frequency-independent CMB structures are well-pronounced at high latitudes.

## 7 ITERATIVE APPLICATION OF FASTICA ON PRE-CLEANED DATA

In Bottino et al. (2008), we introduced the concept of an iterative application of FASTICA to the data. Specifically, we applied the algorithm to sky maps that had already been cleaned using templates with coupling coefficients themselves derived using a FASTICA analysis. Here, we continue the study begun in the previous section by applying such an iterative step as a function of mask to data sets pre-cleaned with coefficients that are also a function of mask. However, we allow the mask utilised to determine the template coefficients to be different to that applied in the iterative phase to the cleaned data, and then investigate the resulting matrix of results. We utilise either the five frequency maps cleaned using the Haslam template, or the Q- V- and W- band data cleaned with either of the putative synchrotron templates (Haslam or K-Ka).

This approach to the problem is interesting in order to study in more detail the limits of application of the algorithm. Specifically we can address two related questions:

- (i) Can an initially poor cleaning of the data be compensated for by the iterative internal analysis of the cleaned data set?
- (ii) Is it possible to derive a full-sky CMB map cleaned of any low-latitude residuals resulting from the application of corrections based on high latitude foreground coefficients? If not, can we determine the minimal mask, that allows reliable extraction of the underlying CMB signal?

In fact, we speculate that the combination of different masks at different stages of the iterative analysis can effectively introduce some sensitivity to the relative mix and spectral variations of the foreground components on the sky.

In our FASTICA implementation, for a blind analysis of  $N$  input sky maps we expect  $N$  returned independent components. One of these will be identified as the CMB sky, the remainder correspond to other physical components on the sky. In figures 5, 6 and 7, we show the spatial distribution of this residual foreground derived as a function of the mask used initially to compute

the template coefficients for cleaning the input sky maps, and of the mask used to subsequently perform the iterative analysis. Each row of the plot corresponds to results derived from maps cleaned with those coefficients determined for a given mask, whilst each column corresponds to results derived when using the stated mask for the iterative analysis. Consequently, the diagonal maps are those returned when the same mask is adopted for the two steps of the analysis.

When the standard masks (ie.  $Kp2$ ,  $Kp0$ ,  $KQ85$ ,  $KQ75$ ) are used in the two steps of the analysis, we find that only one of the additional non-CMB components returned by FASTICA is actually consistent with a foreground residual, the remainder being related to noise and residual dipole terms. A box in the plot highlights these maps which we retain as the most interesting results. Conversely, when either the processing mask is used or a full-sky analysis is performed in one of the two step of the analysis, the cleaned data remain strongly contaminated from the Galactic foregrounds, and there is no clear single map representing foreground residuals. Nevertheless, for completeness, we show representative maps that contain at least part of the strong foreground signal. In some cases, e.g. when the processing mask is used for iterative analysis after data pre-cleaning with the standard templates, there is evidence of consistent residuals with those shown in the red box in figure 5. However, it is not possible to draw strong conclusions from these cases.

If we compare the new 5-year results with the 3-year results from our previous analysis, we can confirm the previous conclusions, which are actually reinforced thanks to the wider set of masks adopted here.

- There is strong evidence of a residual which is concentrated near the Galactic Centre and along the edge of the mask.
- There is a residual associated with the North Polar Spur seen in the Haslam data, clearly visible when all five WMAP frequencies are included in the analysis and the Haslam map is used as the synchrotron template. This oversubtraction of the emission implies a spectral difference between this region and high latitude regions. However, the amplitude falls off when a larger cut is used, which may indicate some variation of this index along the spur's extent.
- The spatial distribution of the contamination is larger when we analyze the K-, Ka-, Q-, V- and W-band data using the Haslam map as the synchrotron template than when only the Q-, V- and W-band maps are input data. Moreover, the amplitude of the residual is also lower in the latter case, implying a spectrum that falls with frequency. Whether the residual is a new physical component of emission or simply a region where the spectral index is flatter than the high latitude areas is unclear.
- The intensity of this component gets even weaker when the K-Ka map is adopted to model the synchrotron emission. This is a consequence of the fact that the K- and Ka-data do contain this emission component which also supports the concept that the use of internal templates such as the K-Ka map, even with a simple global scaling, provides a more accurate means to model the foreground contaminations than from data obtained at much lower or higher frequencies. However, the physical interpretation of such templates is difficult since they are certainly mixtures of several components.

Including the new cases of analysis, where the masks are mixed, other interesting points come out:

1. The processing steps with respect to masking do not commute - for example, the residuals from the iterative analysis using a  $KQ85$  mask applied to maps cleaned by  $Kp2$  coefficients are not identical to the case when the masks are reversed.
2. When the scaling factors are computed with the thinner masks (namely the  $Kp2$  and the  $KQ85$ ), the spatial distribution of the residual is similar regardless of the mask used for the iterative analysis. Therefore, the component is not a simple effect of the cut of the Galactic plane.
3. The algorithm provides a good component separation also when we adopt the coefficients relative to the largest masks: the algorithm is able to recover the residual whose amplitude depends on the mask applied in the second step of the analysis. What is not subtracted in the cleaning process, is actually recovered by the iterative analysis.
4. The residuals associated with the  $Kp0$  coefficients and the K-Ka template seem to show unexpectedly high amplitude compared to smaller cuts and the similar  $KQ85$  mask.
5. The  $KQ75$  coefficients computed with the K-Ka template seem to be the optimal ones in order to clean the data: the residual maps appear uniformly clean. The obvious conclusion would be that they give the most realistic description of the contaminated sky. However, this idea is not always supported by analogous considerations about the CMB component. In fact, the set of coefficients are reliable only when the  $KQ75$  mask is used also for the iteration. In the other cases, FASTICA mixes all the components and part of the residual actually contaminates both the CMB map and a third component, which generally shows a noise pattern.

The last point highlights that a consideration of the residuals revealed by the iterative analysis can actually be misleading, and is not a sufficient figure of merit to quantify the performance of such an analysis by itself. To make such a judgement, we must consider the CMB component returned by the analysis and, in particular, its power spectrum. However, before we make this assessment in section 8, we make a small digression.

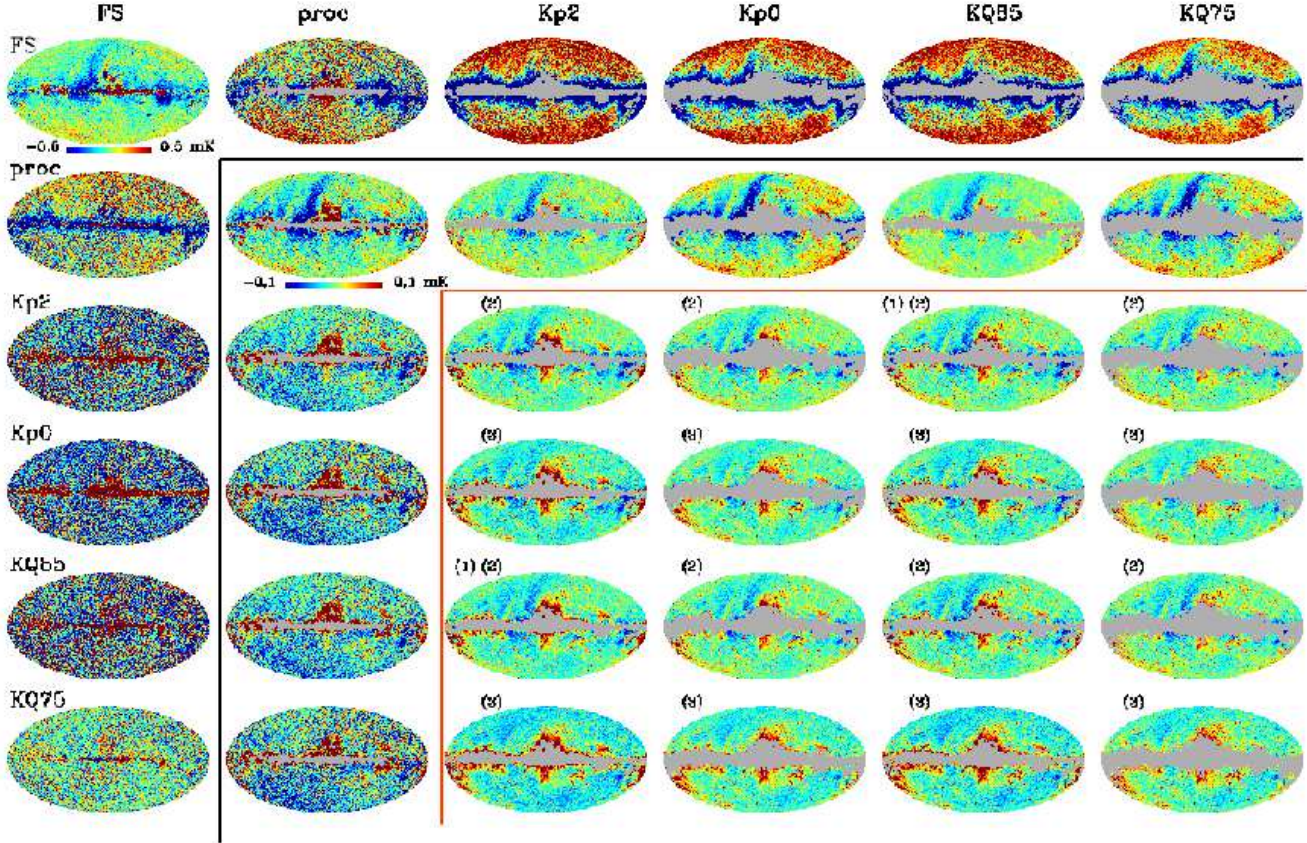


**Figure 5.** Maps of the residual component recovered by FASTICA with the iterative blind analysis of the cleaned K-, Ka-, Q-, V-, and W-band data. Results on a given row are derived from input maps cleaned using coefficients determined for the stated mask; results on a given column are derived when the stated mask is used in the iterative step of the analysis. The labels have the same meanings as figure 3. The numbers over the maps refer to the list of comments in the text. Here, the Haslam map is used as a synchrotron template. The red line highlights the cases where single well-defined residual component is detected. The black line separates regions where different temperature scales have been used for the plots.

### 7.1 Is the foreground residual the ‘WMAP haze’?

Since we cannot simply associate the recovered residual component with any of the standard templates used to describe the diffuse Galactic emissions, we attempt to address the issue of its spatial distribution and physical origin. In fact, Dobler et al. (2008a) have already attempted to give an answer to these questions, and identify the residual (the so-called *WMAP haze*) as a hard synchrotron component, whose origin is linked to dark matter annihilation in the centre of our Galaxy. They also provide a simple model for its spatial distribution, namely:

$$\mathbf{h} \propto \begin{cases} \frac{1}{r} - \frac{1}{r_0} & \text{for } r < r_0; \\ 0 & \text{for } r > r_0, \end{cases} \quad (2)$$

where  $r$  is the angular distance to the Galactic center and  $r_0$  is arbitrarily set equal to 45 degrees.

Examination of the maps returned by FASTICA indicates that a spherically symmetric distribution is not the optimal one to describe the component. Nevertheless, a direct fit of this model to our maps shows a quite good agreement, with a correlation coefficient of 0.45. Therefore, we adopted it as a fourth template and repeated the iterative analysis using the Haslam map as the soft-synchrotron template. A physical interpretation of the coupling coefficients returned by FASTICA is not simple: the values are negative for all the frequencies except the K- and Ka-bands, making a spectral index computation very difficult. Nevertheless, we used the values to clean the data and considered the amount of contamination still present in the residual map from the corresponding iterative analysis. Although these coefficients are representative of the best FASTICA solution when the haze template is used, a negative value adopted to clean the data can effectively correspond to the introduction of a spurious foreground residual in the data. Therefore, we also studied the case where the haze template cleaning was only performed for the K- and Ka-bands; for the remaining frequencies we retained the old three-template coefficients. Figure 8 shows the residual maps obtained in these two cases when the *Kp2* mask is applied to the data together with the previous result derived from the three templates fit of the data.

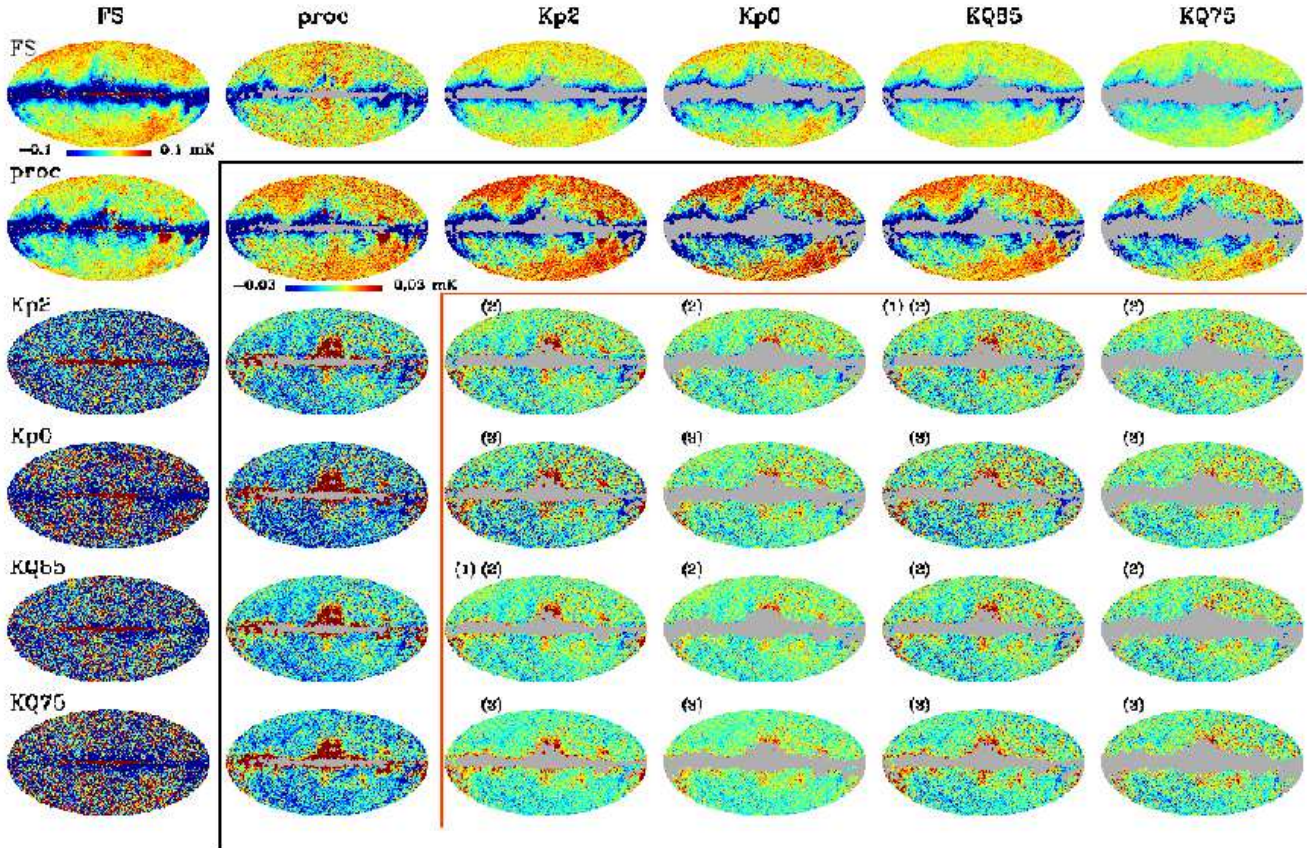


**Figure 6.** Maps of the residual component recovered by FASTICA with the iterative blind analysis of the cleaned data Q, V and W band. Rows and columns have the same meaning as figure 3 as well as the red box and the numbers, and again the Haslam map is used as the synchrotron template.

When the haze template is employed, bright emission around the Northern extension of the Galactic Centre is still present, whilst the Southern hemisphere emission is essentially removed. There is little obvious difference between the two cases. Some refinement of the haze model is still required.

## 8 POWER-SPECTRUM EVALUATION OF ITERATIVELY CLEANED MAPS

Note that, in what follows we will use the *WMAP* team’s 5-year power spectrum derived from the V- and W-band data using the MASTER algorithm over all angular scales<sup>4</sup> as a canonical reference. This should not imply that the result is indisputable, nevertheless several independent analyses have yielded results in good agreement. Moreover, we will make comparisons on a qualitative level regarding the broad features of the spectrum, rather than make detailed inferences about cosmological parameters.

In figure 9, we show the CMB maps obtained when the five *WMAP* bands are cleaned using the coefficients determined from an analysis when the Haslam map is employed as the synchrotron template: we chose this case as the best example to comment on, since it connects to further analyses described later on. We divide a description of the results into two sections – the first dealing with more conventional analysis when only partial skies are analysed, the second considering cases when the signal for the full sky is utilised in at least part of the analysis.

### 8.1 Partial-sky analysis

Generally, with all the possible combinations of coefficients and masks, we obtain CMB maps whose power spectrum is highly consistent with the best estimation of *WMAP*. In figure 10 we have plotted a subset of all possible power spectra computed by our iterative methodology. The selection was carried out on the basis of a reduced  $\chi^2$ -value computed relative to the

<sup>4</sup> Private communication: G. Hinshaw (2009)

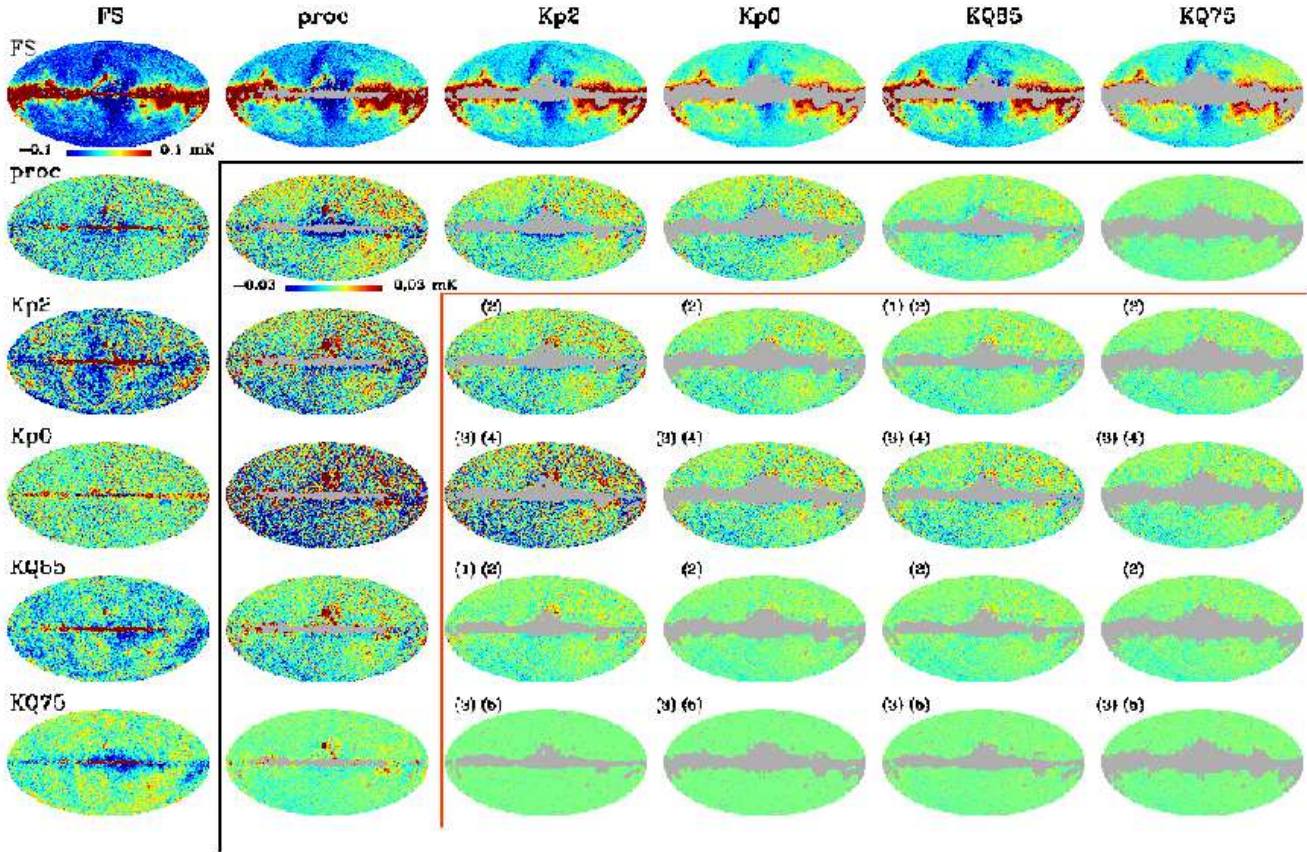


Figure 7. As figure 6 but using the K-Ka map as the synchrotron template.

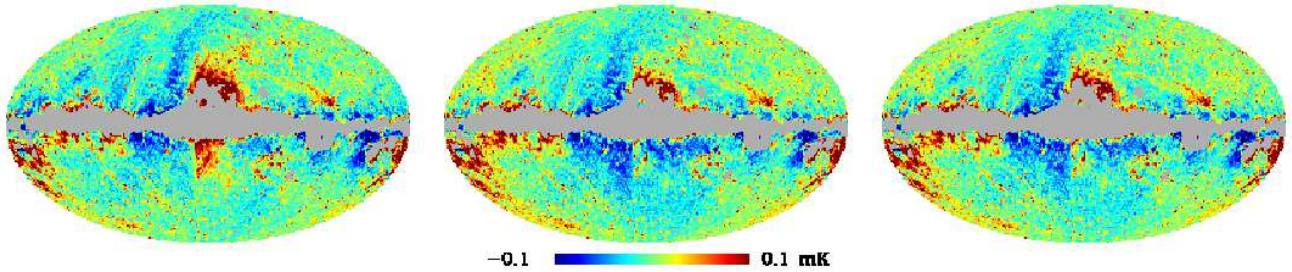
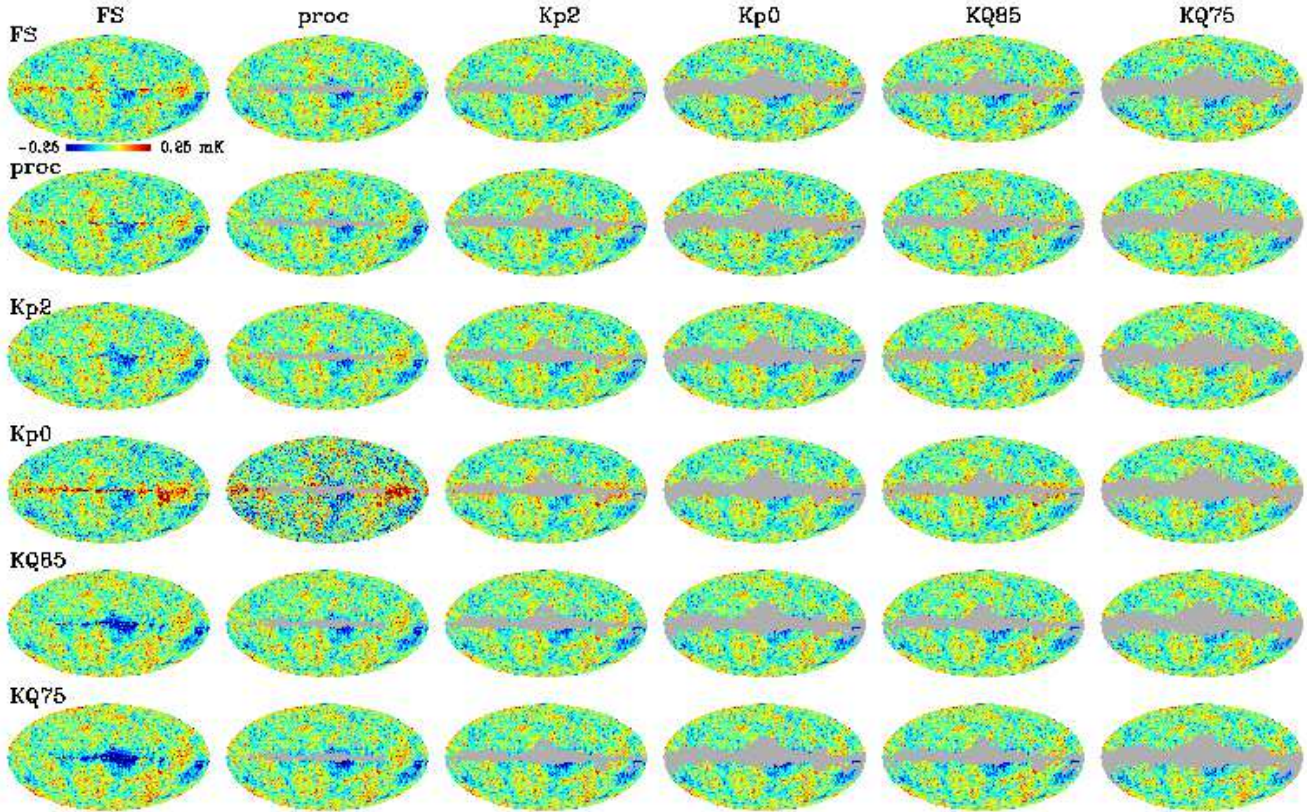


Figure 8. Maps of the residual component recovered by FASTICA with the iterative blind analysis of the cleaned data. These are produced using the coupling coefficients obtained from the templates fit where the haze template is not used (left), when it is added as a fourth template (center) and when the haze coefficients are only used to clean the the K- and Ka-band maps. The Haslam map is adopted as the synchrotron model.

*WMAP* spectrum, and we show some best (top panels) and worst (bottom panels) cases. Note that all plotted power spectra are corrected for the contributions of the instrumental noise (determined using simulations) and the unresolved point sources following Wright et al. (2008).

The values of the  $\chi^2$ -statistic are generally driven by the low ( $\ell < 6$ ) and high multipoles ( $\ell > 250$ ). In order to exclude the possibility that such excesses seen in the power spectra could be associated with an underestimation of the noise, we implemented a cross-power spectrum estimator. Such a method requires two input CMB sky estimates, which we derived using subsets of the individual DA sky maps. For Q- and V-bands, the split is unambiguous since there are only two DAs per frequency. For the W band, we averaged W1 with W2 and W3 with W4. Finally, since for the K-band we have only one differential assembly, two independent inputs were created from averaged maps of the first, second and third year of observations and the fourth and fifth year, respectively. The inverse has been done for the Ka band where the same problem exists. The effect of these selections is to approximately balance the noise properties of the input maps for the power spectrum





**Figure 9.** CMB components recovered by FASTICA when the cleaned *WMAP* data are used as input maps. The data are cleaned according to the scaling factors obtained using the Haslam map as synchrotron template, the  $p$  function and *all* the masks. The iterative analysis itself has been performed with all the different cuts of the sky and the five maps. Each row is referred to the mask adopted to compute the coefficients, further used to clean the data. Inside the row, the single map is obtained from the internal analysis and using a specific mask, whose name is indicated on the top of each column.

evaluation. For each of the two sets of maps, the individual frequencies were then combined with the coefficients derived from the standard analysis, and the cross-power spectrum evaluated. In all cases, this has confirmed the auto-power spectrum estimation after noise correction. Therefore, the excess likely reflects contamination from foreground residuals at low latitude, arising from an inability of the FASTICA algorithm to disentangle the components. This contamination is probably due to the different extension of the masks used to clean the maps and to internally analyse them.

However, given this interpretation, some anomalies are difficult to explain. We would expect the contamination to be larger when the  $Kp2$  and  $KQ85$  masks are used for the internal analysis, yet the  $KQ85$  mask returns a CMB map with a lower contamination than for  $Kp0$ . Moreover, following this logic, we would expect the processing mask provided by the science team of *WMAP* to exhibit the most pronounced excess at high  $\ell$ , but on the contrary it is very small. This suggests that the component separation is mostly driven by specific features of what appears as the residual, rather than simply by its angular extension. This interpretation is also appropriate to explain the results obtained from the maps cleaned using the  $Kp0$  mask coefficients and then analysed with the processing cut. The CMB component returned by FASTICA has a power spectrum which is consistently higher than the other cases, with a larger noise contribution at high multipoles.

## 8.2 Full-sky analysis

As a further experiment, we wanted to test the limits of the applicability of the algorithm by performing a component separation study on *full-sky* maps. In practice, by full-sky we mean the remaining sky coverage after exclusion of the point sources. This experiment is interesting in order to see if FASTICA is able to function satisfactorily, even when the different sources are strongly mixed with each other, as they clearly are in the Galactic plane.

In the first stage of the analysis, we find that the component separation based on template fits is poor. This is only to be expected, since the spectral behaviour of the foregrounds traced by the templates has well-established differences at low- and high-latitude, and since the bright emission from the Galactic plane is likely to drive the fit coefficients. We find that the coefficients are very large for the dust and free-free emissions, but small for the synchrotron radiation. The latter factor

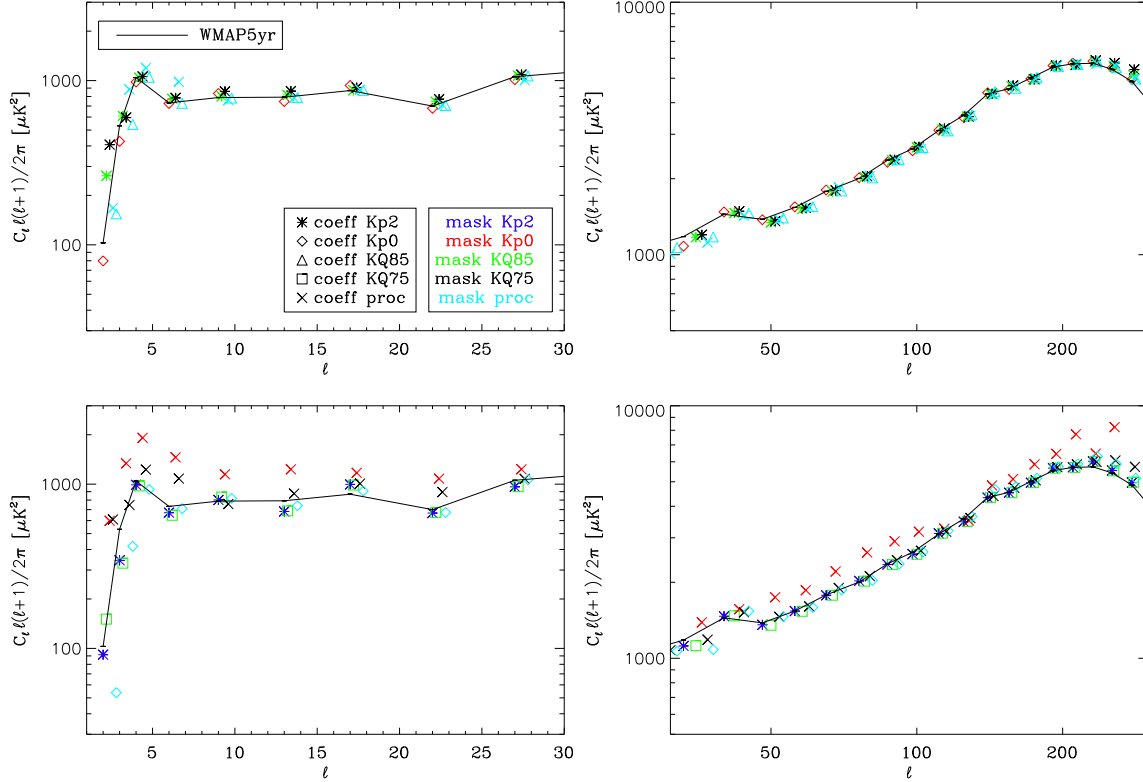


**Figure 10.** Subset of the power spectra of the CMB components recovered by an iterative application of FASTICA when the cleaned *WMAP* data are used as input maps. The data are cleaned according to the scaling factors obtained using the Haslam map as synchrotron template, the  $p$  function and *all* the masks. The iterative analysis itself has been performed with all the different cuts of the sky and the Q, V and W maps. For an input set of maps cleaned using coefficients determined for a specific mask, best- (top row) and worst-case (bottom row) spectra are chosen from the corresponding iterative analyses for all possible analysis masks using a  $\chi^2$  statistic relative to the best-fit *WMAP* spectrum. For clarity, the left column shows the results at low- $\ell$  on a linear scale, the right column shows the intermediate and higher- $\ell$  values on a logarithmic scale.

probably reflects the degree of mixing between the sources, which is particularly strong between the synchrotron and free-free emissions. However, the general trends in spectral behaviour are maintained, and we adopt the coefficients to clean the data as usual.

After the iterative step, the final recovered full-sky CMB map shows clearly extraneous features along the Galactic plane, as shown in the top left corner of figure 9. The corresponding power spectrum (see figure 11) shows, accordingly, a substantial excess on almost all angular scales. Note that the enhancement on small scales ( $\ell > 250$ ) is in the regime limited by the  $1^\circ$  resolution of the analysis. Nevertheless, although we do not wish to over-emphasise its significance, it is likely indicative of foreground residuals.

The cleaned full-sky maps (top-row of figure 9) were also iteratively analysed using the usual set of masks to exclude the Galactic plane. In these cases, we find that, on application of a mask, the excess of power at intermediate and high multipole values largely disappears, confirming that most of the previously observed excess is connected to the spurious structures along the Galactic plane, at latitudes smaller than  $\sim 5^\circ$ . Indeed, the processing mask itself is already sufficiently large to produce this result.

Finally, we have internally analysed the full-sky maps cleaned utilising the coefficients computed using a mask (leftmost column of figure 9). As expected, the data appear strongly contaminated in the Galactic plane region, since the scaling factors describe the properties of the high-latitude sky outside of a specific cut. An intriguing result is constituted by the difference in the nature of this residual contamination as a function of mask: for the high-latitude cuts, there is generally a negative region in the Galactic plane, except when using the *Kp0* mask which retains positive Galactic plane structure. This again suggests anomalous behaviour for those results derived using this mask, following that described in section 5 and further discussed in

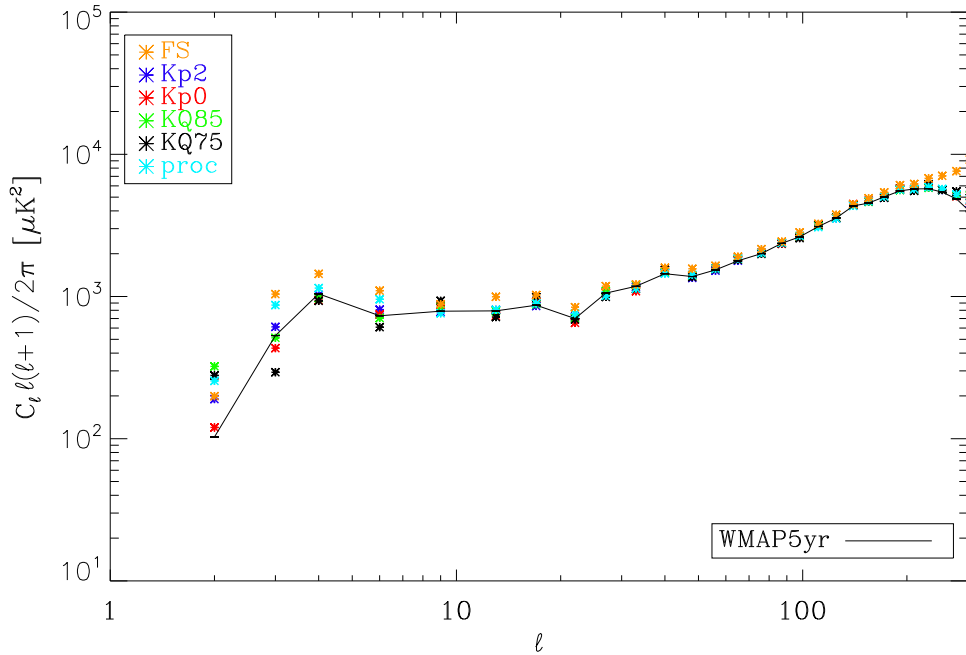


**Figure 11.** Power Spectra of the CMB components recovered by FASTICA applied to the data cleaned according with the coefficients obtained with a full-sky analysis. The Haslam map is adopted as synchrotron template and the coefficients were computed with the  $p$  function. The iterative analysis itself has been performed on all the five maps.

section 5.1, dedicated to the spectral index estimation. The consequence of the existence of this contamination is again an excess at high values of  $\ell$  in the CMB power spectra, which extends to intermediate scales most notably when using the  $Kp0$  and  $KQ75$  masks. None of the spectra can be considered compelling for cosmological purposes.

## 9 APPLICATION OF FASTICA ON WMAP DATA AND TEMPLATES SIMULTANEOUSLY

From what has been presented in the previous section, we conclude that the experimental full-sky analysis does not satisfy our expectations. This happens for two reasons: first of all, we lose information on the foreground components because the template fit is poorly behaved; secondly, the CMB reconstruction shows significant contamination, preventing its use in cosmological studies. However, we did not abandon the idea of producing an adequate full-sky CMB estimation, and considered a data set comprising the ensemble of multi-frequency maps dominated by the CMB component, simultaneously analysed with foreground templates. We considered different combinations of the input data: the five *WMAP* maps were analysed together with the dust and free-free maps, and afterward also including the Haslam map as synchrotron template. The same was done with only the Q- V- and W-band maps: in this case, when the synchrotron template was involved, we used both the Haslam and K-Ka maps. Finally, we considered the five *WMAP* frequency channels alone, in order to quantify the advantages of including foregrounds models.

In figure 12, we show the CMB maps obtained with this new implementation of the algorithm. Unsurprisingly, it appears that the higher the number of input maps, the greater the precision of the CMB map reconstruction. In particular, with all five *WMAP* maps and the three foreground templates, we obtained the best CMB map with respect to those recovered in all the other combinations of input data. Spurious structures along the Galactic Plane are clearly visible in all the maps, while in this case they get much weaker and are perhaps even confined to the inner part of the Galaxy. Quantitatively speaking, we checked the impact of these structures on the power spectrum, shown in figure 13. The CMB map returned with the largest number of input data is the most consistent with the best estimate from the *WMAP* 5-year data, even though at high  $\ell$  values there is still an excess of power, which is clearly the consequence of these residuals.

However, we focused our attention on the map obtained from the combination of the largest data set, computing as usual the power spectrum as a function of applied mask. This analysis, shown in figure 14 seems to confirm that the excess is related to structures observed along the plane since it disappears with more extensive cuts. Moreover, in figure 15 we compared its

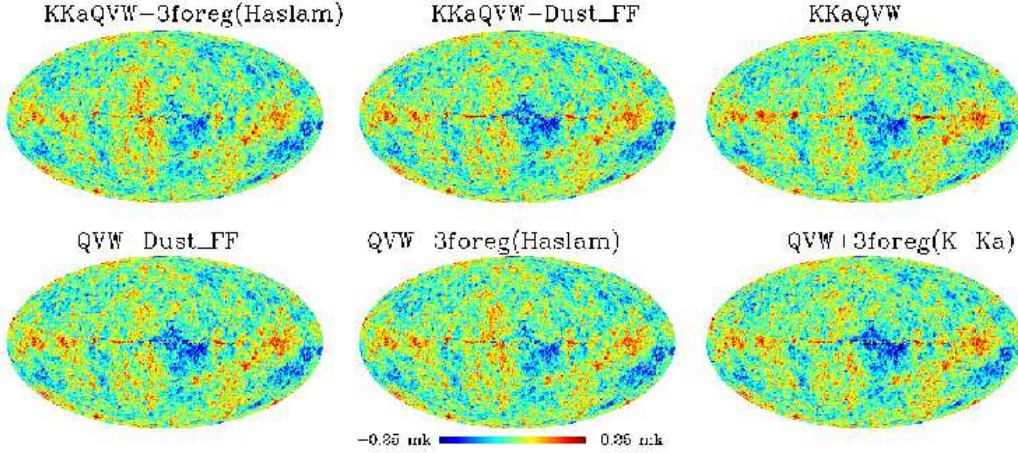


**Figure 12.** CMB maps returned by FASTICA when applied on different combination of data. Several cases have been considered: i) the *WMAP* maps at the K-, Ka-, Q-, V- and W-bands together with three foregrounds templates, where the Haslam map is used to describe the synchrotron emission; ii) the *WMAP* maps at the K-, Ka-, Q-, V- and W-bands together with the dust and free-free templates; iii) the *WMAP* maps at the K-, Ka-, Q-, V- and W-bands; iv) the *WMAP* maps at the Q-, V- and W-bands with the dust and free-free templates; v) the *WMAP* maps at the Q-, V- and W-bands together with three foregrounds templates, where the Haslam map is used to describe the synchrotron emission; v) the *WMAP* maps at the Q-, V- and W-bands together with three foregrounds templates, where the K-Ka map is used to describe the synchrotron emission. The cleanest map is the one obtained from the first case considered, but generally spurious structures are visible along the Galactic Plane in all the maps.

power spectrum to those of the CMB maps derived with the internal full-sky analysis of the cleaned data. The aim of this exercise was to verify that the new implementation of FASTICA was an improvement on previous attempts.

The excess of power for  $\ell > 200$  is smaller than in the other cases of comparison, even though the difference is not marked and we are at the limit of the multipoles range imposed by the data angular resolution of  $1^\circ$ . On the other hand, however, at intermediate values of the multipoles, it is more consistent with the *WMAP* best estimation, while the other power spectra are slightly higher in amplitude.

Ultimately, we want to compare the FASTICA method with the results of other methods currently used to achieve the same aim. We considered the ILC map produced by the *WMAP* science team (Gold et al. 2009), a similar foreground-reduced map in which the frequency dependent weights were determined in harmonic space by Kim et al. (2008) (hereafter HILC) and a further alternative obtained by Delabrouille et al. (2008) using needlets as the basis of the analysis (hereafter NILC). Since these techniques make use of the *WMAP* data alone without any augmentation by internal templates, we revert to the fully blind analysis also performed for the *WMAP* three-year data in Maino et al. (2007), and consider the case when all five frequency bands are used. Again, the power spectrum has been chosen as the figure of merit to compare the performances of these methods. These are shown in figure 16. We have used published information to compute the noise correction to the spectra based on simulations, except in the NILC case where a correction has been directly provided, though here no correction for unresolved point sources has been made. The power spectra of the HILC and the NILC maps are the most consistent with the *WMAP* best estimation, whereas the ICA map seems to be the most contaminated with residuals, since it shows the largest excess of power on small angular scales. However, in some sense, the comparison is unfair towards FASTICA since the other methods allow some regional dependence of the weights used to form the optimal CMB estimate, either by solving for coefficients in different regions of the sky separately, or finding a best spatially varying set of weights.

In conclusion, the ICA approach affords a fair estimate of the CMB signal, although improvements are still possible. However, at this stage, we simply took advantage of this result to address another question.

### 9.1 What is the minimal mask?

Given the imperfections of our full-sky CMB map reconstruction, we are forced to apply a cut in order to use it to extract cosmological information. We therefore took the opportunity to define the minimal mask required by FASTICA to recover a non-contaminated CMB map.

In order to determine the mask, we first implemented the *WMAP* thresholding method used to generate the *Kp2* and *Kp0* masks as described by Bennett et al. (2003), but here applied to the FASTICA map. However, we found that, given the relatively low amplitudes of the residuals, pixels for a given threshold set soon included likely genuine CMB structures, which then contaminated the mask. Consequently, we considered simple parallel cuts of different latitude extension. Finally, we

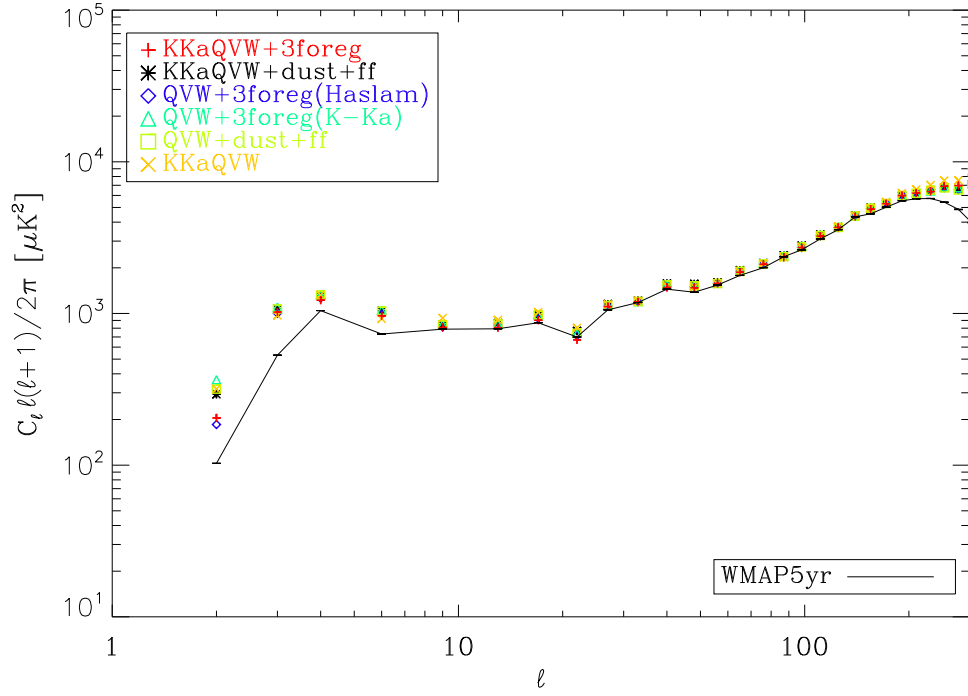


Figure 13. Full-sky power spectra of the CMB maps shown in figure 12.

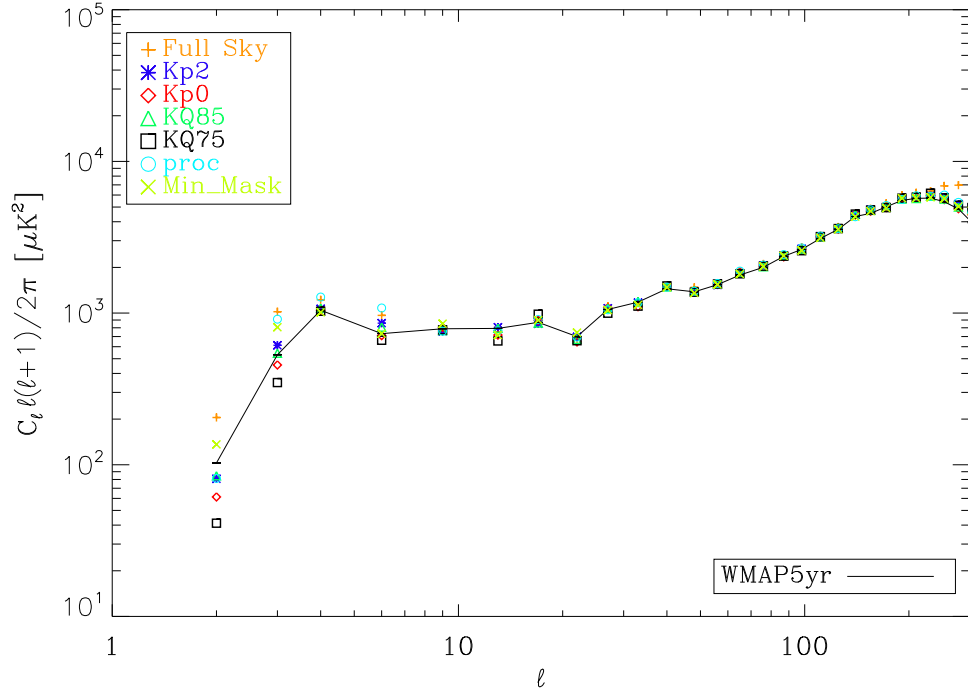
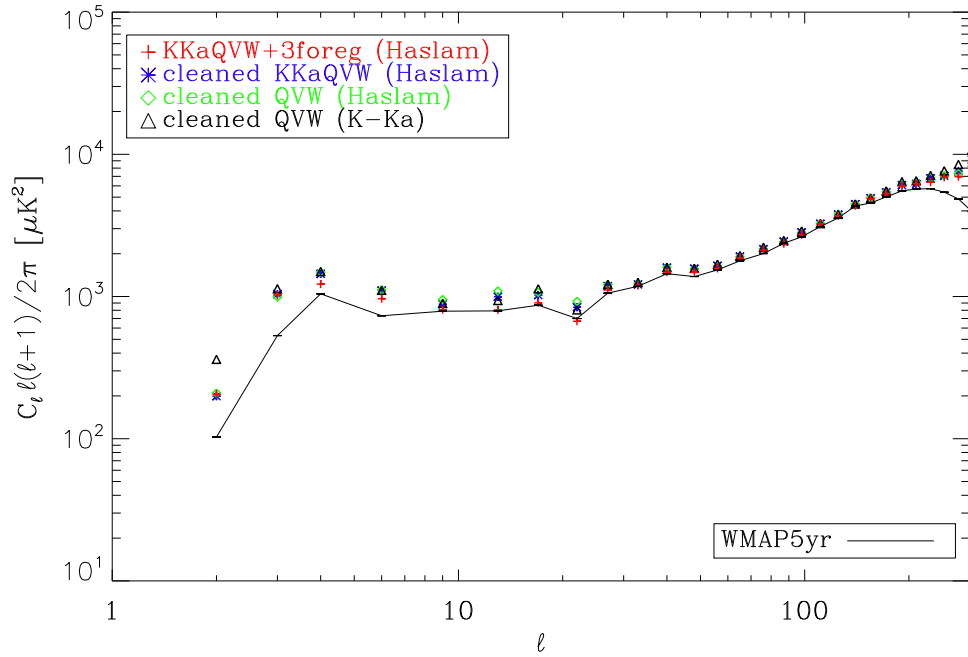
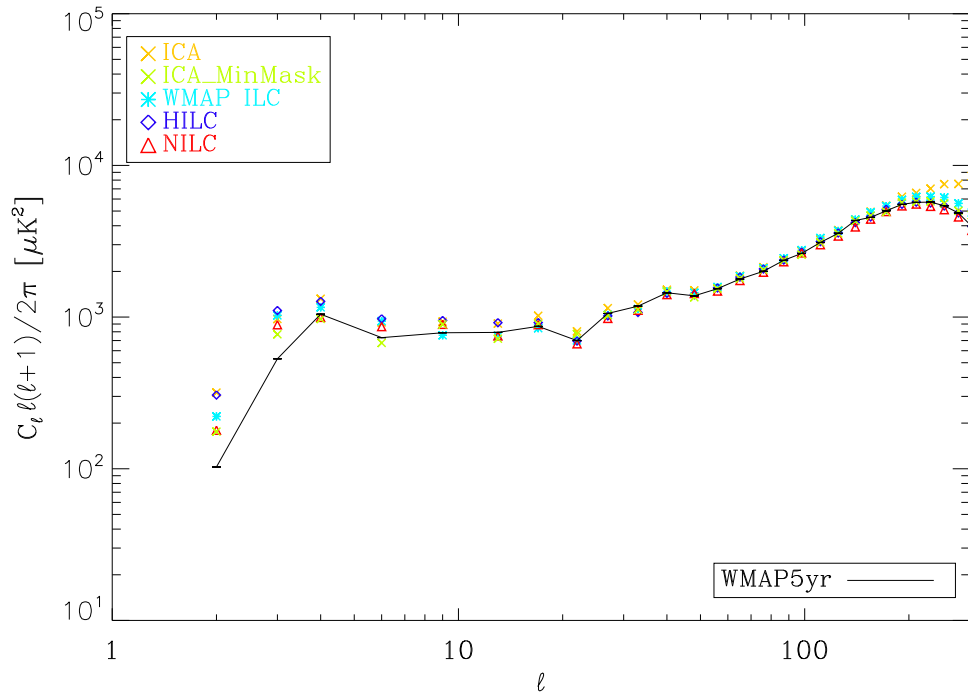


Figure 14. Power spectra of the CMB map (KKaQVW+3foreg in figure 12) returned by a full-sky FASTICA analysis when applied simultaneously to the five WMAP maps together with three foregrounds templates. We used the Haslam map as synchrotron template and the  $p$  function. Power-spectra are then evaluated after applying a variety of masks.



**Figure 15.** Comparison of the power spectrum of the CMB recovered from the simultaneous full-sky analysis of the *WMAP* data together with the templates and those obtained with the simultaneous internal analysis of the cleaned data. We show all the different combinations of the input data internally analysed. The results are obtained using the  $p$  function.



**Figure 16.** Power spectrum of our best full-sky map obtained with FASTICA, compared with those of the *WMAP* ILC map, the HILC map produced by Kim et al. (2008) and the NILC map of Delabrouille et al. (2008).

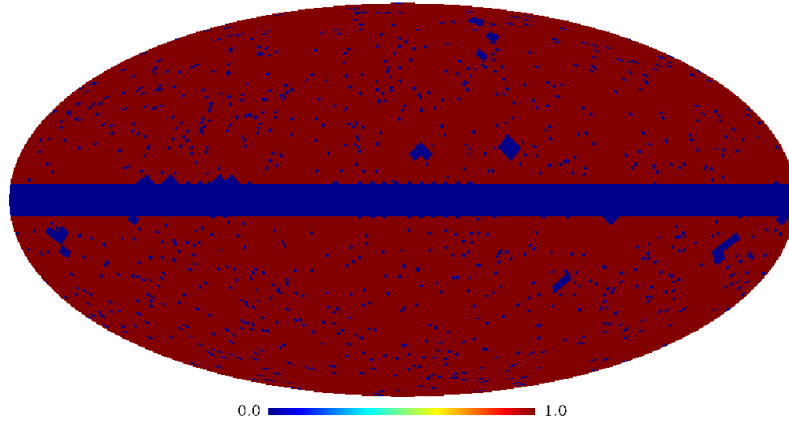


**Figure 17.** Minimal mask derived from the FASTICA simultaneous analysis of the five full-sky *WMAP* data with the three foreground templates. It is basically the combination of the processing mask and a parallel cut of the regions of the Galactic plane with  $|b| < 6^\circ$ . As usual we also excluded the point sources, according with the mask provided by the *WMAP* science team.

determined a minimal mask, which is the union of the processing mask and a parallel cut of the regions with  $|b| < 6^\circ$ . As usual, we also excluded the point sources, according to the mask provided by the *WMAP* science team. The result is shown in figure 17. Figures 14 and 16 then show the power spectra derived from the *WMAP* data either including or excluding the three foreground templates respectively for this mask. In both cases, the agreement with the *WMAP* spectrum is impressive over all  $\ell$ , with the remaining differences being on large angular scales.

## 10 DISCUSSION

In this paper, we have undertaken a foreground analysis of the *WMAP* 5-year data using the FASTICA algorithm, as previously applied to the *WMAP* 3-year data in Bottino et al. (2008). Various improvements in the implementation have allowed us to address several open questions from our previous work, and allowed some experimentation with the technique.

We used the code to perform a foreground fit of the data on a frequency-by-frequency basis, where the Galactic components are described by all-sky templates obtained at wavelengths where the corresponding emission mechanisms dominate. Specifically, we adopted the Finkbeiner et al. (2003)  $H\alpha$ -map as a template for the free-free emission, the Finkbeiner et al. (1999) FDS8 model for thermal dust emission, and the 408 MHz radio continuum all-sky map of Haslam et al. (1982) as utilized in the first year *WMAP* analysis for the synchrotron emission. In the latter case, we have also considered the differenced of the *WMAP* K- and Ka-band data, as preferred in their 3-year analysis.

The first step of the analysis is the computation of the coupling coefficients, which give an estimation of the contamination of the foreground emission level in the data. We know already that these coefficients depend on the extension of the mask used to exclude the most contaminated regions of the Galactic plane. We further investigated this dependence, thanks to the new *KQ85* and *KQ75* masks provided by the *WMAP* science team. We confirmed the result which reinforces the idea of a spatial variation of the foreground emissions. Moreover, it suggests the component separation is driven by some key regions, rather than the extension of the mask itself. On the other hand, we reestablish some anomalies obtained when the *Kp0* mask is adopted that remain unexplained.

We have considered the spectral behaviour of the derived scaling factors when the Haslam et al. (1982) data is used as the synchrotron template, since an interpretation of the analogous results derived using the K-Ka template is compromised by the fact that it is itself a mixture of foreground components. We evaluated the spectral index for the synchrotron emission, the anomalous dust-correlated component, and the free-free emission. In the first two cases, we found steeper, though statistically consistent, spectral behaviour as compared to previous analysis, e.g. Davies et al. (2006).

We then focused our attention on the estimation of the free-free spectral index. A non-trivial dependence of the spectral behaviour on the extension of the mask confirms what was already found with the *WMAP* 3-year data. However, an understanding of the behaviour is probably associated with two factors – the spatial variation of the physical properties of the component (e.g. electron temperature which directly relates to the scale-factor associated with the  $H\alpha$  template) which is mostly linked to specific structures close the Galactic plane, and the connection of the statistical properties of the foreground with the response of the algorithm as a function of the non-linear function used. The spectral behaviour is generally flat and even increasing with frequency, if the  $p$  function is used together with the *KQ85* and *KQ75* masks. We have interpreted these

spectral features as a consequence of a self-similarity of the Gaussian/non-Gaussian mixtures at each frequency. When the  $g$  function is adopted, a more uniform behaviour, consistent with theoretical expectations, is obtained. Finally, in both the cases, the  $Kp0$  mask gives a steeper spectral index than the expected value of 2.14. We note that none of our results are compatible with the existence of a bump in the spectrum, as claimed by Dobler et al. (2008b) and subsequently explained by the existence of spinning dust in the WIM that is traced morphologically by the  $H\alpha$  template.

A more extensive approach to the cleaning of the data has been introduced in connection with the iterative application of FASTICA. A set of coefficients obtained with a specific mask is used to remove the foreground contaminations in the maps, which are then internally analysed with *all* the Galactic cuts available. This new approach allowed us to check the capability of the iterative step to recover from a poor initial cleaning of the data and still yield a credible CMB estimate. A useful figure of merit for the quality of the results is then the corresponding CMB power spectrum as compared to the *WMAP* estimation. In general, the iterative approach is very robust, although some not completely satisfactory results provide a evidence of limitations of the algorithm. Specifically, it seems that the algorithm provides poorer estimates of the CMB if applied on smaller regions of the sky.

Associated with the iterative analysis, we were able to determine the presence of a residual foreground whose spatial distribution is concentrated along the Galactic plane, with pronounced emission near the Galactic center. The extension of this residual is independent of the mask used, meaning that it is not just the effect of a poor component separation. However, it decreases in amplitude if the K and Ka band are not included in the input data set, and more so if the K-Ka map is used to compute the synchrotron coefficients. This indicates that the component has a falling spectrum with frequency, but whether it is a new physical component or simply a manifestation of a region with different spectral behaviour from the average is difficult to determine. In any case, it does confirm the utility of the K-Ka data as a better template to describe the low-frequency foreground mixture. In fact, this emission was already observed in the SMICA analysis of Patanchon et al. (2005) and is clearly consistent with the *WMAP* haze of Finkbeiner et al. (2004). The putative model of its spatial distribution proposed by Dobler et al. (2008a) is found to be in reasonable agreement with the data, although some refinements are required.

Finally, we attempted a full-sky analysis of the same data set. Even though the code then challenged to work in regions of the sky where the cross-talk among the components is very high, we find that FASTICA is still able to achieve good results, particularly based on the iterative analysis of the cleaned data as originally implemented in Bottino et al. (2008). We focused our attention on the CMB reconstruction, comparing the results with those produced by a simultaneous analysis of the multi-frequency *WMAP* data with the templates. In this case, the result is slightly better. On the other hand, a direct comparison of the power spectra of the ICA CMB map with variants of the ILC approach proposed recently (HILC, NILC) suggests the need to include more spatial dependence in our analysis. Indeed, the excess of power observed on small angular scales is likely the signature of some residual structures along the Galactic plane. Consequently, to partially compensate for such structures, we defined a minimal mask to be used in a practical analysis of the derived CMB map. The resulting FASTICA power spectra for our preferred data sets then agree remarkably with the best estimate of the CMB spectrum provided by the *WMAP* team.

## ACKNOWLEDGMENTS

Some of the results in this paper have been derived using the HEALPix (Górski et al. 2005) package. We acknowledge the use of the Legacy Archive for Microwave Background Data Analysis (LAMBDA). We thank Gary Hinshaw for providing the best-fit *WMAP* power spectrum derived from the V- and W-band data using the MASTER algorithm over all angular scales. Support for LAMBDA is provided by the NASA Office of Space Science. We acknowledge the use of Craig Markwardt's fitting package MPFIT<sup>5</sup>.

## REFERENCES

- Baccigalupi, C. et al. , 2004, *MNRAS* , 354, 55  
 Banday A.J. et al. , 2003, *MNRAS* , 345, 897  
 Bennett C.L. et al. , 2003, *Astrophys. J. Supp.* , 148, 97  
 Bonaldi, A., Ricciardi, S., Leach, S., Stivoli, F., Baccigalupi, C., de Zotti, G., 2007, *MNRAS* , 382, 1791  
 Bottino, M., Banday, A.J., Maino, D., 2008, *MNRAS* , 389, 1190  
 Cardoso, J.F., Martin M., Delabrouille J., Betoule M., Patanchon G., ArXiv e-prints, 0803.1814  
 Chiang, Lung-Yih, Naselsky, P. D., Coles, P., 2009, *Astrophys. J.* , 694, 339  
 Davies R.D., Dickinson C., Banday A.J., Jaffe T.R., Górski K.M., Davis R.J., 2006, *MNRAS* 370, 1125  
 Delabrouille, J., Cardoso, J.F., Patanchon, G. 2003, *MNRAS* , 346, 1089

<sup>5</sup> <http://cow.physics.wisc.edu/~craigm/idl/fitting.html>



- Delabrouille, J., Cardoso J.F., Le Jeune M., Betoule M., Fay G., Guilloux F., 2008, submitted to *Astron. & Astrophys.*
- Dickinson C., Davies R.D., Davis R.J., 2003, *MNRAS* , 341, 369
- Dobler, G., Finkbeiner D.P., 2008, *Astrophys. J.* , 680, 1222
- Dobler, G., Finkbeiner D.P., 2008, *Astrophys. J.* , 680, 1235
- Dobler, G., Draine, B.T., Finkbeiner D.P., 2009, *Astrophys. J.* , submitted
- Draine B.T., Lazarian A., 1998b, *ApJ*, 508, 157
- Eriksen, H. K., Jewell, J.B., Dickinson, C., Banday, A. J., Grski, K. M., Lawrence, C. R., 2008, *Astrophys. J.* , 676, 10E
- Finkbeiner D.P., Davis, M., Schlegel D.J., 1999, *Astrophys. J.* , 524, 867
- Finkbeiner D.P., 2003, *Astrophys. J. Supp.* , 146, 407
- Finkbeiner D.P., 2004, *Astrophys. J.* , 614, 186
- Gold, B. et al. , 2009, *Astrophys. J. Supp.* , 180, 265
- Górski, K.M., Hivon, E., Banday, A.J., Wandelt, B.D., Hansen, F.K., Reinecke, M., & Bartelmann, M., 2005, *Astrophys. J.* , 622, 759
- Hansen, F.K., Banday, A.J., Eriksen, H.K., Górski, K.M., Lilje, P.B., 2006, *Astrophys. J.* , 648, 784
- Haslam C.G.T. et al. , 1982, *Astron. & Astrophys. Suppl.* , 47, 1
- Hyvärinen A., 1999, *IEEE Signal Processing Lett.* , 6, 145
- Hyvärinen A. & Oja E., 2000, *Neural Networks* , 13, 411
- Hinshaw G. et al. , 2007, *Astrophys. J. Supp.* , 170, 288
- Hinshaw G. et al. , 2009, *Astrophys. J. Supp.* , 180, 225
- Kim J., Naselsky P., Christensen P.R., 2008 *Phys. Rev. D* 77, 103002
- Maino D. et al. , 2002, *MNRAS* , 334, 53
- Maino D., Donzelli S., Banday A.J., Stivoli F., Baccigalupi C., 2007, *MNRAS* , 374, 1207
- Park, C.-G. Park, C. Gott, J. R., 2007, *Astrophys. J.* , 660, 959
- Patanchon G., Cardoso J.F., Delabrouille, J., Vielva P., 2005, *MNRAS* , 364, 1185
- Tegmark, M., de Oliveira-Costa, A., Hamilton, A. J., 2003, *PRD*, 68, 123523
- Wright, E. L., Chen, X., Odegard, N., Bennett, C. L., Hill, R. S., Hinshaw, G., Jarosik, N., Komatsu, E., 2008, arXiv:0803.0577
- Ysard, N., Mivilles-Deschenes, M-A., Verstraete, L., 2009, arXiv:0906.3360v2